

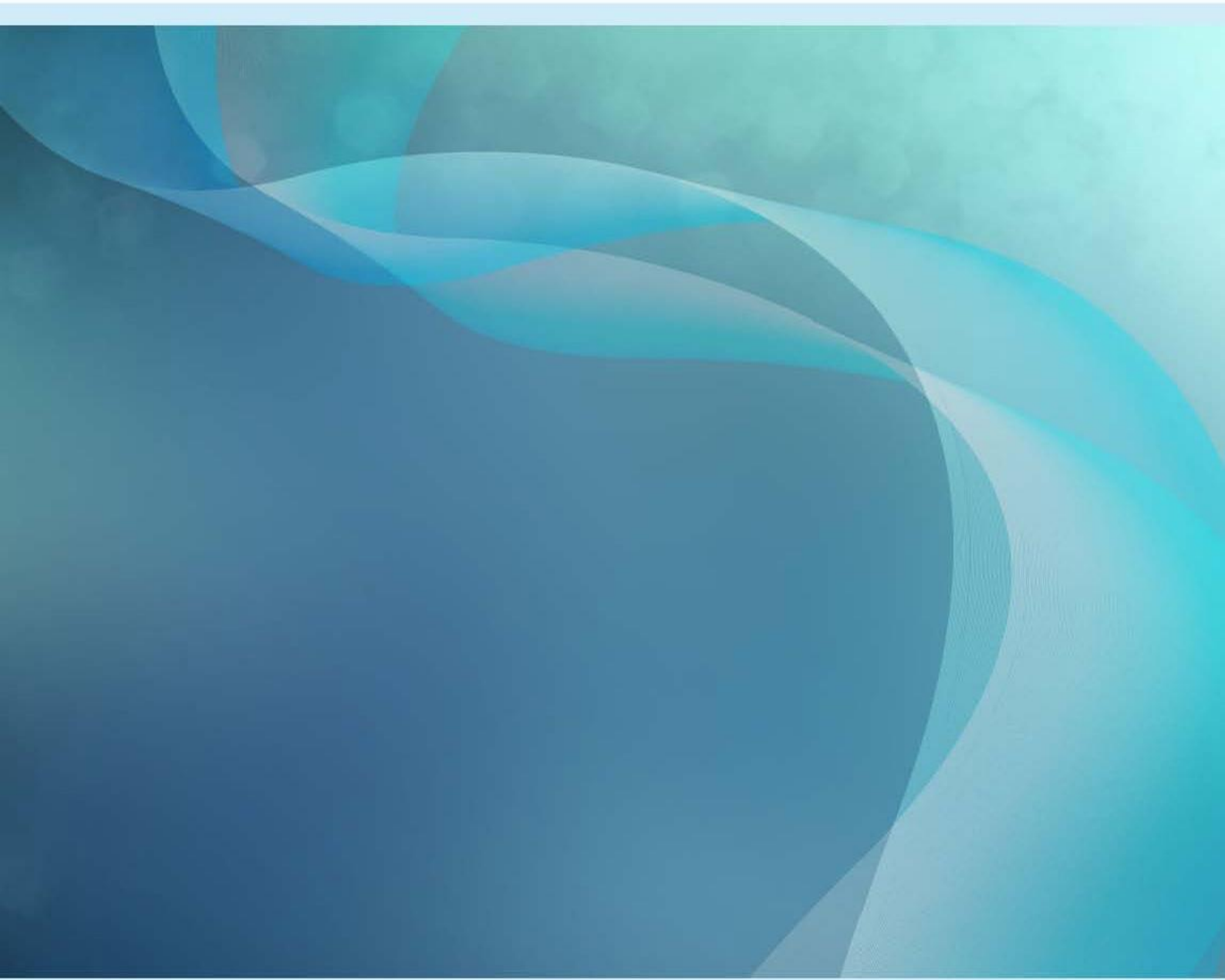


Australian Government

Bureau of Meteorology

The Australian Landscape Water Balance model (AWRA-L v7)

Technical Description of the Australian Water Resources Assessment Landscape model
version 7



Citation: Frost, A. J., and Shokri, A., (2021) The Australian Landscape Water Balance model (AWRA-L v7). Technical Description of the Australian Water Resources Assessment Landscape model version 7. Bureau of Meteorology Technical Report.

Version number/type	Date of issue
1.0.6	30/08/2021

© Commonwealth of Australia 2021

This work is copyright. Apart from any use as permitted under the Copyright Act 1968, no part may be reproduced without prior written permission from the Bureau of Meteorology. Requests and inquiries concerning reproduction and rights should be addressed to the Production Manager, Communication Section, Bureau of Meteorology, GPO Box 1289, Melbourne 3001. Information regarding requests for reproduction of material from the Bureau website can be found at www.bom.gov.au/other/copyright.shtml

Published by the Bureau of Meteorology

Contact details

Dr. Andrew Frost

a/Team Lead

Hydro-informatics & Surface observations, Research Program, Science and Innovation Group

Bureau of Meteorology

PO Box 413, Darlinghurst NSW 1300

Tel: +61 2 9296 1517

Email: Andrew.Frost@bom.gov.au

Dr. Ashkan Shokri

Senior Hydrologist

Hydro-informatics & Surface observations, Research Program, Science and Innovation Group

Bureau of Meteorology

PO Box 1289, Melbourne Vic 3001

Tel: +61 3 9669 4303

Email: Ashkan.Shokri@bom.gov.au

Water Sector email

Water Sector Program, Business Solutions Group

Email: water@bom.gov.au

Summary

This technical report provides a detailed description of the Bureau of Meteorology's operational Australian Water Resources Assessment Landscape model: AWRA-L version 7. The report includes a description of:

- the overall conceptual structure,
- the model components (water balance, atmospheric vapour fluxes, energy balance, and vegetation phenology), and
- how the model was parameterised nationally.

This report details the recent model and structural changes implemented in AWRA-L version 7. Process equations are provided along with a brief background on their choice and individual parameterisation.

The AWRA-L version 7 is used to produce outputs on the operational Australian Landscape Water Balance website www.bom.gov.au/water/landscape and the model code is available via the Bureau of Meteorology's AWRA Community Modelling system (<https://github.com/awracms/awra cms>).

The model performance against observations and benchmarking against other models are summarised in a companion report (Frost et al. 2021).

A reference guide for parameters used in the model code and within this document is provided in Appendix A.

Table of Contents

1	Introduction	1
1.1	The AWRA Modelling System.....	1
1.2	Differences between AWRA-L v6 and AWRA-L v7	2
1.2.1	Daily Climate and static spatial Inputs.....	3
1.2.2	Structural/conceptual model changes:	3
1.2.3	Calibration Process	4
1.2.4	Conceptual structure	4
1.3	Structure of this report.....	6
1.4	Spatial data and Hydrologic Response Units (HRUs)	7
1.4.1	Input climate data	7
1.4.2	Static spatial datasets	10
1.4.3	HRU proportions ($f_{grass}, f_{imp}, f_{tree}$)	11
2	Water balance	14
2.1	Water balance equations	15
2.1.1	Surface runoff ($QR = Qh + Qs$)	16
2.1.2	Soil storage ($S0, Ss, Sd$), drainage ($D0, Ds, Dd$) and interflow ($QIF = QIO + QIs$)	17
2.1.3	Groundwater storage (Sg) and fluxes (Qg, Eg, Y)	21
2.1.4	Total Streamflow and surface water storage	25
3	Vapour fluxes and the energy balance	27
3.1	Potential evaporation $E0$	27
3.2	The energy balance	28
3.2.1	Upward and Downward shortwave radiation	28
3.2.2	Upward longwave radiation	29
3.2.3	Downward longwave radiation.....	29
3.3	Actual evapotranspiration ($Etot$)	30
3.3.1	Interception evaporation (Ei)	30
3.3.2	Soil evaporation (Es)	31
3.3.3	Evaporation from groundwater (Eg)	31
3.3.4	Root water uptake from ($Et = Us + Ud$)	31
3.3.5	Transpiration from groundwater (Y)	35
4	Vegetation Phenology	37
5	Parameterisation.....	40
5.1	Parameterisation of AWRA-L v7.....	40
5.1.1	Calibration and evaluation approach	40
5.1.2	Calibration and validation data	40
6	Conclusion	46
	References	47
	Appendices.....	51
	Appendix A: Table of model variables.....	52
	Appendix B: Downward longwave radiation derivation.....	56

List of Tables

Table 1. AWRA-L v5 and v6 parameter values. Values that apply to either the deep or shallow rooted HRU (or both) are provided. Values that are optimised are shown in bold.	45
Table 2. List of variable names used in this document and the corresponding variables used in the model code. Units are those given in this document.	52

List of Figures

Figure 1. Conceptual AWRA-L grid cell with key water stores and fluxes shown	5
Figure 2. AWRA-L conceptual structure. Purple: climate inputs; Blue rounded boxes: water stores; Red boxes: water flux outputs; Brown: energy balance; Green rounded boxes: vegetation processes. Dotted line indicates HRU processes.	7
Figure 3. AWRA-L v5 Wind speed climatology (u2)	8
Figure 4. Fraction shallow-rooted, impervious, and deep-rooted areas within each grid cell ..	13
Figure 5. AWRA-L hydrological processes. Blue rounded boxes indicate water storages, white if no storage, white boxes are water balance fluxes, and red boxes are the output fluxes.	14
Figure 6. Continental distribution of reference precipitation Pref	17
Figure 7. Saturated conductivity (Kxsat) and proportion available water capacity (SsAWCSsmascale) for the top (0), shallow (s) and deep (d) soil layers.	20
Figure 8. Average slope β within a grid from a 3 second DEM	21
Figure 9. Groundwater drainage coefficient (Kg)	22
Figure 10. Effective porosity n	24
Figure 11. Hypsometric curve conversion of groundwater storage to fraction of cell saturated and fraction of cell available for transpiration	25
Figure 12. Streamflow routing coefficient (Kr)	26
Figure 13. (a) Foliage Projective Cover FPC and (b) Maximum possible root water uptake from the deep soil store (Udmax_hrudr).....	33
Figure 14. Vegetation height of deep-rooted vegetation hveg	35
Figure 15. Maximum Leaf Area Index (LAI_{max})	39
Figure 16. Location of unimpaired catchments used for model evaluation with climate zones overlain.	42

List of Acronyms

AVHRR:	Advanced Very High Resolution radiometer
AMSR-E:	Advanced Microwave Scanning Radiometer for the Earth Observing System
ASRIS:	Australian Soil Resource Information System
AWAP:	Australian Water Availability Project
AWRA-L:	Australian Water Resources Assessment Landscape Model
AWRA-R:	Australian Water Resources Assessment River Model
AWRAMS:	Australian Water Resource Assessment modelling system
BoM:	Bureau of Meteorology
CMRSET:	CSIRO MODIS reflectance-based Scaling ET
CSIRO:	Commonwealth Scientific and Industrial Research Organisation
ET:	Evapotranspiration
fPAR:	fraction of Photosynthetically Active Radiation absorbed by vegetation
FPC	Foliage projected cover
GRACE	Gravity Recovery and Climate Experiment
HRU:	Hydrological Response Unit
LAI:	Leaf Area Index
NWA:	National Water Account
MODIS:	Moderate Resolution Imaging Spectroradiometer
MTTPT:	Maximum Tree Transpiration per Tree Basal Area
RWI:	Regional Water Information
TBA:	Tree Basal Area
WIA:	Water in Australia
WIRADA:	Water Information Research and Development Alliance

1 Introduction

The Australian Water Resources Assessment (AWRA) Modelling System underpins the Bureau of Meteorology's (herein the Bureau) water information services for national water resource assessment reporting, water use accounting and situation monitoring. The modelling system has been developed by the Bureau and CSIRO over the last decade and is run operationally at the Bureau to provide both situational awareness and national retrospective water resource assessment.

The AWRA-L (landscape) model runs on a daily timestep and 0.05° grid (approximately 5 km) simulating the landscape water balance for Australia from 1911 to yesterday. Key outputs from the AWRA-L model include surface runoff, soil moisture, evapotranspiration and deep drainage. Outputs from the model are available through the website interface (<http://www.bom.gov.au/water/landscape>); or on request as a registered user.

AWRA-L is optimised to the whole water balance using a national streamflow dataset along with satellite derived soil moisture, vegetation cover, terrestrial water storage, and evapotranspiration estimates. The model is further validated against a wide range of observational datasets including point scale soil moisture probe data, flux tower estimates (of evapotranspiration and soil moisture) and groundwater recharge estimates (Frost et al., 2021). The modelling system was released in 2016 as a community modelling system (<https://github.com/awracms/awra cms>), enabling application and development by the wider research community.

Operational AWRA-L modelled outputs have been made publicly available since November 2015 (using AWRA-L version 5) and the modelled fluxes have been used internally and externally for various climatological, flood, drought, fire, water and agriculture applications across Australia. This document describes AWRA-L version 7 released operationally by the Bureau in 2021.

1.1 The AWRA Modelling System

The AWRA Modelling System underpins the Bureau water information services that are mandated through the Water Act (2007). The science of the AWRA Modelling System (see Vaze *et al.*, 2013; Elmahdi *et al.*, 2015; Hafeez *et al.*, 2015); has been developed since July 2008 through the Water Information Research and Development Alliance (WIRADA) between CSIRO and the Bureau. The AWRA Modelling System has been operational at the Bureau since 2011-12 for regular use in the National Water Account (NWA) and Water Resources Assessment reports.

The Bureau's has been regularly interacting with a wide range of stakeholders about their needs and how these can be met by a daily operational water balance model. These interactions have spanned Commonwealth agencies and State government water and agriculture agencies, catchment management authorities, water utilities, consultants, water industry professionals, research organisations, universities, and farmers.

This technical report describes the AWRA-L v7 model structure and is intended to be used as a quick reference for the model equations and processes used in the Bureau's AWRA Modelling system (both the operational system run by the Bureau and the supporting community modelling system code). This document relies heavily on the following descriptions of prior AWRA-L versions:

- **AWRA-L v0.5:** Van Dijk, A. I. J. M. (2010c) *The Australian Water Resources Assessment System. Technical Report 3. Landscape Model (version 0.5) Technical Description.*
- **AWRA-L v5:** Viney, N., Vaze, J., Crosbie, R., Wang, B., Dawes, W. and Frost, A. (2015) *AWRA-L v5.0: technical description of model algorithms and inputs.* CSIRO, Australia.
- **AWRA-L v5:** Frost, A. J., Ramchurn, A., and Smith, A. (2016b). *The Bureau's Operational AWRA Landscape (AWRA-L) Model.* Bureau of Meteorology Technical Report.
- **AWRA-L v6:** Frost, A. J., Ramchurn, A., and Smith, A. (2018) *The Australian Landscape Water Balance model (AWRA-L v6). Technical Description of the Australian Water Resources Assessment Landscape model version 6.* Bureau of Meteorology Technical Report

Limited explanation is provided here for the derivation and choice of parameterisations. Van Dijk (2010a) provides the original design principles and the rationale for choice of the original national parameterisation in v0.5. Viney *et al.* (2015) describes the improvements that have been made in parameterisation and the conceptual structure of AWRA-L v5. Frost *et al.* (2018) reported updates in relation to climate inputs (solar radiation and wind), static spatial inputs (fraction deep-rooted vegetation within each grid cell, hypsometric curves, soil storage and drainage properties), soil drainage equations, and calibration objective function applied in AWRA-L v6. This document updates the details of the model according to changes incorporated in AWRA-L v7.

1.2 Differences between AWRA-L v6 and AWRA-L v7

The changes implemented within version 7 have been made based on experimentation and improved performance along with improved functionality across three broad areas:

- Improved static and dynamic inputs,
- Altered conceptual structure and improved model equations,
- Altered calibration approach and/or inputs.

This section summarises those changes. The overall improved performance is detailed in the AWRA-L v7 evaluation report (Frost *et al.*, 2021)

1.2.1 Daily Climate and static spatial Inputs

Climate data alignment: Some climate inputs (solar radiation and maximum temperature) have been shifted to align more closely with the AWRA-L output timestep (see section 1.4.1).

Actual vapour pressure (p_e): AWRA-L v7 uses p_e as a temporally dynamic input. This differs from AWRA-L v6 and previous versions where p_e was calculated based on input daily minimum temperature grids (see section 1.4.1).

Average daily temperature: Previously the weighted mean of the daily maximum (T_{max}) and minimum (T_{min}) temperature with the weights, equal to 0.75 and 0.25 was used. This was optimized respectively to 0.85 and 0.15 in the version 7 (see section 3.1).

Hydrological Response Unit proportions (f_{grass} , f_{tree} and f_{imp}): the static maps defining the fraction of shallow, deep and new impervious Hydrological Response Units (HRUs) spatially have been updated (see section 1.4.3) according to the mapping described in Vaze et al (2018).

Soil storage and drainage properties: Static spatial maps for the saturated hydraulic conductivities $K_{x_{sat}}$ and the (proportional) available water holding capacity $S_{x_{AWC}}$ of the soil layers, where $x = 0$: top 0-10cm, $x = s$: shallow 10-100cm, and $x = d$: deep 100-600cm have been updated according to the mapping described in Vaze et al (2018).

Maximum root water uptake from the deep soil: A map of foliage projected cover (derived from satellite imagery) is now used to estimate tree basal area and resulting deep-rooted vegetation maximum root water uptake (using a calibrated regression relationship, see section 3.3.4). This replaces a constant spatial value across the continent.

Vegetation height of deep-rooted vegetation: The top of the tall vegetation canopy, was updated (see section 3.3.4) based on new spatial grids derived from lidar estimates as described in Vaze et al (2018).

1.2.2 Structural/conceptual model changes:

Additional impervious Hydrological response unit: A new impervious surface HRU has been added to the existing shallow and deep-rooted vegetation HRUs. The impervious HRU comprises urban landscapes and naturally impervious areas, with the HRU mapping described in Vaze et al (2018). The HRU has no infiltration into the soil profile and the canopy rainfall interception storage is zero because there is no vegetation on the impervious areas (see section 1.4.3).

Soil drainage equations: A modified equation for top layer soil drainage has been included to improve top layer (0-10cm) soil moisture variability. The equation averages the saturated conductivity of the soil layer and the layer below according to a

calibratable parameter, rather than using an a priori specified value as in previous versions of AWRA-L (see section 2.1.2).

Groundwater baseflow equations: A threshold has been added above the lowest topographical point within a cell to cut-off baseflow from groundwater storage enabling ephemerality of streamflow in certain locations, along with improving streamflow bias (see section 2.1.3).

1.2.3 Calibration Process

Several changes were applied towards a more robust parameterisation of the model:

Updated catchment streamflow: Updating of catchment boundaries and streamflow data used in calibration and verification according to the Bureau's geofabric version 3 and water data online. This improves the overall quality of the calibration (see section 5.1).

Satellite derived vegetation fraction using Moderate-resolution Imaging Spectroradiometer (MODIS) and **terrestrial water storage** using Gravity Recovery and Climate Experiment (GRACE) were added as calibration variables, along with streamflow and satellite derived soil moisture and evapotranspiration. This provides better constraints for the overall model calibration according to the water balance and vegetation components (see section 5.1).

Updated satellite soil moisture and evapotranspiration: Newly updated 8-day CMRSET MODIS based evapotranspiration (replacing monthly data) and ASCAT satellite based soil moisture (replacing AMSRE data) was used in calibration (see section 5.1).

A new spatial calibration approach: The calibration process and objective function now reflects the spatially distributed satellite data being used, rather than lumped/average catchment evaluation of objectives. That is, the gridded satellite data is compared to the AWRA-L grid equivalent data, rather than a catchment average value. This allows better evaluation of spatial variability (see section 5.1).

1.2.4 Conceptual structure

AWRA-L (Van Dijk, 2010c; Viney *et al.*, 2014; Viney *et al.*, 2015; Frost *et al.*, 2016b; Frost *et al.*, 2018) is a one dimensional, 0.05° grid based water balance model over the continent that has semi-distributed representation of the soil, groundwater and surface water stores. Within each grid cell there are three soil layers (top: 0-10cm, shallow: 10cm-100cm, deep: 100cm-600cm) and three hydrological response units (HRU: shallow rooted, deep-rooted, and the new impervious landscapes, Figure 1). The first two layers combined is also called the root-zone soil layer (0-100cm).

Key fluxes and stores output by AWRA-L as output of the [operational Australian Landscape Water Balance website](#) include runoff, actual evapotranspiration, soil

moisture for the three soil layers (Top 0-10cm, Shallow 10cm-100cm, and Deep 100cm-600cm soil) and deep drainage to the groundwater store - Figure 1.

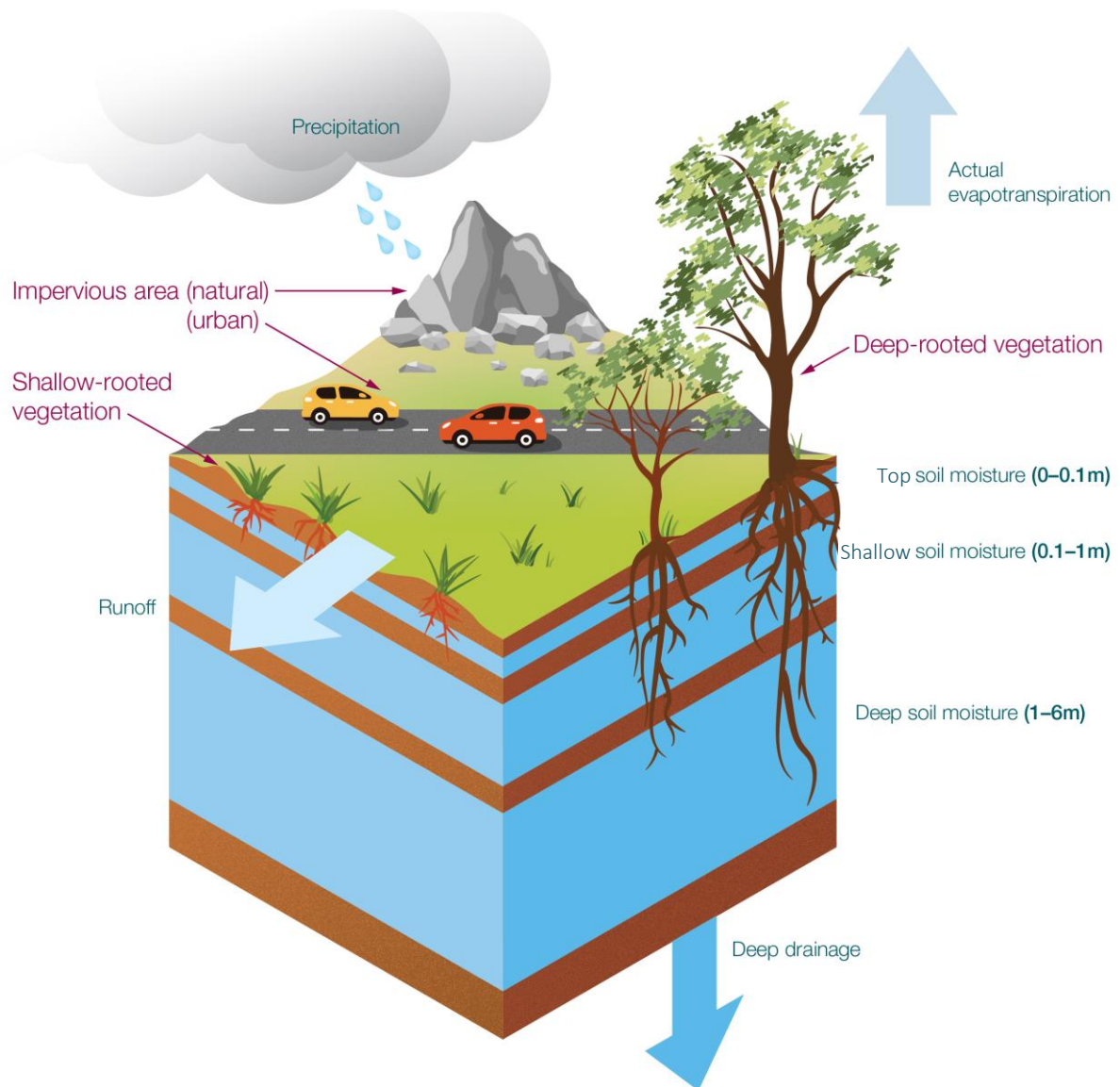


Figure 1. Conceptual AWRA-L grid cell with key water stores and fluxes shown

The hydrological processes AWRA-L models are:

- partitioning of rainfall between interception losses and net rainfall,
- saturation excess overland flow (depending on groundwater store saturation level),

- infiltration and Hortonian (infiltration excess) overland flow,
- saturation, interflow (lateral flow), drainage from soil layers,
- soil evaporation from top soil moisture store and transpiration from shallow and deep soil moisture stores, and
- baseflow, evaporation and transpiration from the groundwater store.

The soil layers are modelled separately for 3 hydrological response units (HRU): (a) grass: shallow rooted vegetation with depth 1m, (b) trees: deep-rooted vegetation with depth 6m and (c) impervious landscapes with root depth equal to zero.

The following vegetation processes are modelled for the shallow rooted and deep rooted HRUs:

- transpiration, as a function of maximum root water uptake and optimum transpiration rate; and
- vegetation cover adjustment, as a function of the balance between the theoretical optimum and the actual transpiration, and at a rate corresponding to vegetation cover type.

Hydrologically, the HRUs differ in their aerodynamic control of evaporation, interception capacities, degree of access to different soil layers, and infiltration rate. Groundwater and river water dynamics are simulated at grid cell level and hence parameters are uniform across the grid cell, and dynamic variables (e.g., fraction groundwater saturated area and open water within stream channels) are equal between HRUs. Figure 2 shows the conceptual structure of AWRA-L.

1.3 Structure of this report

This report is structured according to spatial data required, the three functional components of the model shown in Figure 2, and then how the model is parameterised:

- Section 1.4: Spatial data and Hydrologic Response Units
- Chapter 2: Water balance
- Chapter 3: Vapour fluxes and the energy balance
- Chapter 4: Vegetation phenology
- Chapter 5: Parameterisation

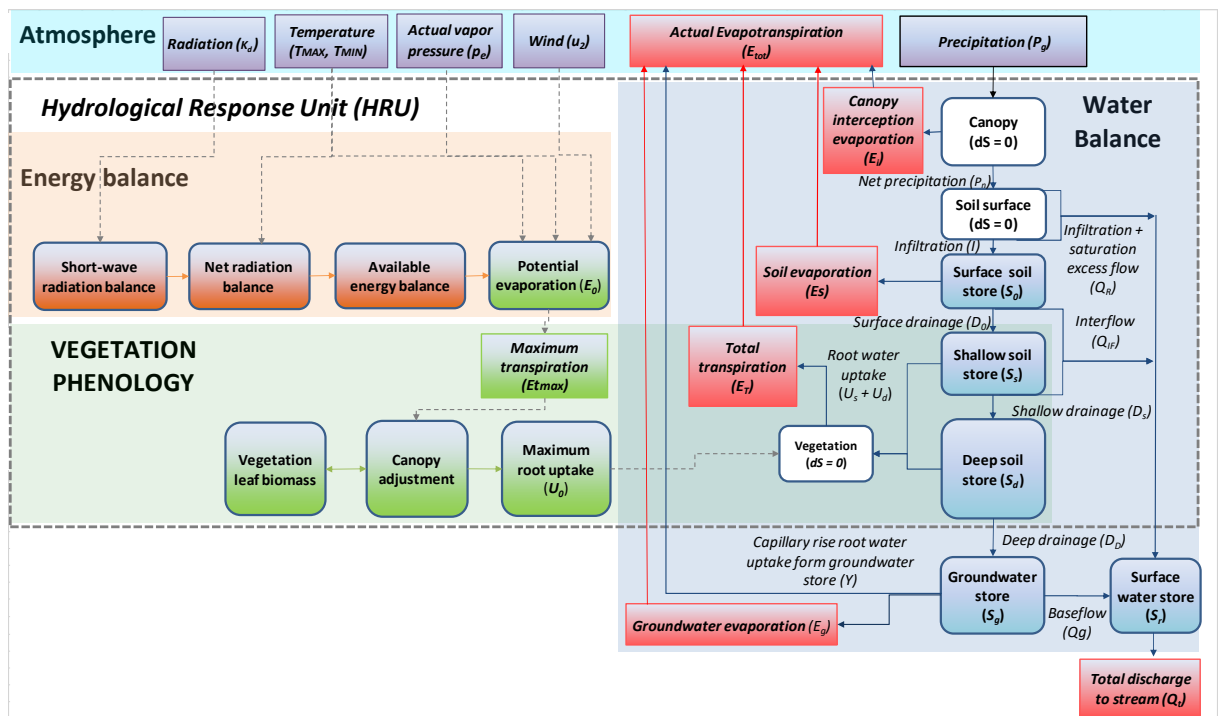


Figure 2. AWRA-L conceptual structure. Purple boxes: climate inputs; Blue boxes: water stores; Red boxes: water flux outputs; Brown: energy balance; Green boxes: vegetation processes. Dotted line indicates HRU processes.

1.4 Spatial data and Hydrologic Response Units (HRUs)

1.4.1 Input climate data

The spatial resolution of AWRA-L is driven by the resolution of input climate data, namely 0.05° (approximately 5 km).

AWRA-L uses the daily [Australian Gridded Climate Data \(AGCD\) v1 Australian Water Availability Project \(AWAP\)](#) climate data set that consists of air temperature (daily minimum and maximum) and daily precipitation from 1st January 1911 to yesterday (Jones et al., 2009).

The rainfall and temperature data are interpolated from station records and provided on a 0.05° grid across Australia. Additionally, daily solar exposure (downward shortwave radiation) is produced from geostationary satellites (Grant et al. 2008) and aggregated to the same 0.05° AWAP grid. The solar radiation record is from 1990 to yesterday, with the Himawari-8 satellite used since 23rd March 2016. Prior to that date

the GMS-4, GMS-5, GOES-9 and MTSAT-1R satellites were used. Daily climatological averages (taken for each month) are used for solar radiation prior to 1990.

Spatially interpolated site based daily wind run observations are used for daily average wind speed from 1975 onwards, when sufficient site observations were collated by the Bureau (see McVicar *et al.*, 2008 for details of the interpolation approach). A daily varying wind speed climatology value is used, based on the period 1975-2017 when there is no data available (ie. prior to 1975). This differs from AWRA-L v5 and previous versions where this daily data was averaged temporally to generate a single daily average value that applied at all timesteps (Figure 3).

To improve the model accuracy, p_e has been added to the temporally dynamic inputs of AWRA-L v7. Until AWRA-L v6, the actual vapour pressure (p_e) was calculated inside the model by assuming the daily minimum temperature as the dewpoint. Similarly to rainfall and temperature, p_e data is interpolated from station records based on temperature data and is provided on a 0.05° grid across Australia (Jones *et al.*, 2009). As actual vapour pressure is provided in gridded form for 9 am and 3 pm nationally, a weighted average was used as the input to the model to reflect the average daily value. The weight is a new parameter for AWRA v7 with an optimum value found to be 0.2 for the 9:00 am and 0.8 for the 3:00 pm values.

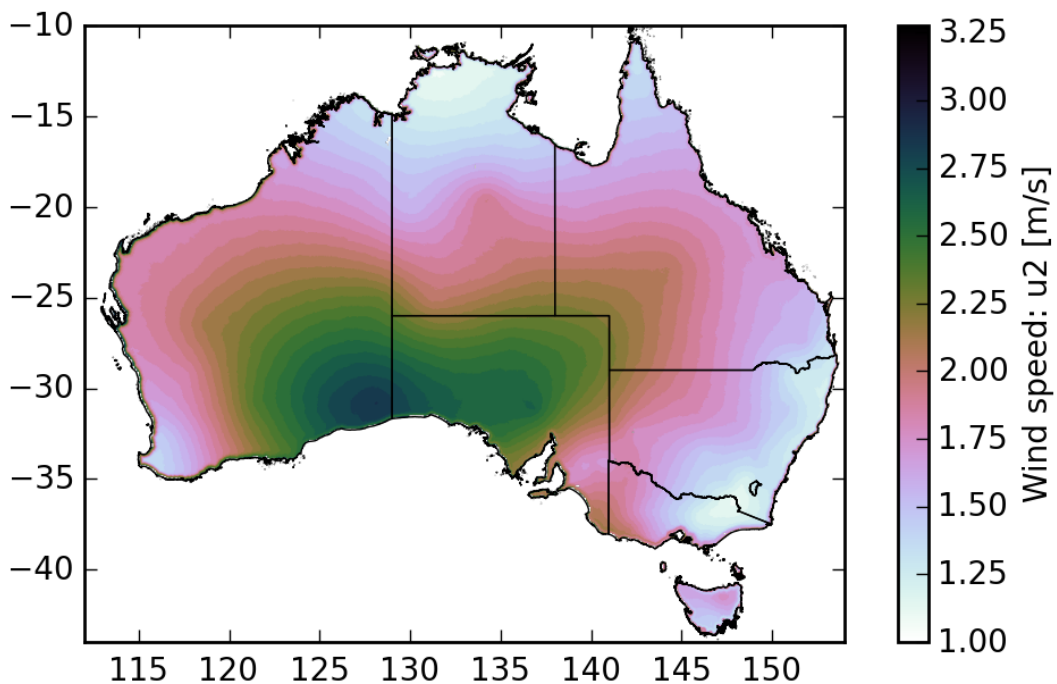


Figure 3. AWRA-L v5 Wind speed climatology (u_2)

The following notation is used for the climate forcing in this report:

- P_g Daily gross precipitation to 9am local time [mm],
- K_d Daily downwelling shortwave (solar) radiation midnight to midnight [$\text{MJ m}^{-2} \text{d}^{-1}$],
- u_2 Wind speed at a height of 2 m to 9am [m/s],
- p_e Actual vapour pressure [Pa],
- T_{min} Daily minimum air temperature to 9am local time [$^{\circ}\text{C}$], and
- T_{max} Daily maximum air temperature from 9am local time [$^{\circ}\text{C}$].

AWRA-L calculates the water balance between 9 am of the day before to 9 am of its timestamp, predominantly to align with the observational period of rainfall. However, the minimum and maximum temperature of a given date corresponds to two differing 24-hour periods (the minimum value corresponds to the 24 hours before 9 am and the maximum temperature corresponds to the 24 hours after 9 am). Further, the solar measurements are the average values from midnight to midnight for a given date, with daylight predominantly aligning with the 24 hours ending 9am the following day. The actual vapour pressure is measured at 9 am and 3 pm, and we use a weighted average of these values to correspond to the day following 9am. As a result, the input data is shifted as follows to represent the 24 hours to 9am used to timestamp AWRA-L outputs:

- P_g – as is (dated same as AWRA-L outputs)
- K_d – shift forwards 1 day
- T_{max} – shifted forwards 1 day
- T_{min} – as is (dated same as AWRA-L outputs)
- u_2 – as is (dated same as AWRA-L outputs)
- p_e – shifted forwards 1 day

The shifting of T_{max} and K_d was implemented for the first time in AWRA-L v7 to fit with the 9 am to 9 am day.

A weighted average of the daily minimum and maximum air temperature values is taken to get an average temperature value to calculate Potential Evaporation, with the T_{min} being set to T_{max} in cases where $T_{min} > T_{max}$ – see section 3.1.

1.4.2 Static spatial datasets

Static spatial datasets are used to parameterise AWRA-L spatially. These spatial grids (discussed subsequently within the document) are as follows:

$f_{grass}, f_{imp}, f_{tree}$ f_{grass} is the proportion of shallow rooted vegetation in each cell (left panel of Figure 4). f_{imp} is the proportion of impervious landscapes (centre panel Figure 4), f_{tree} is the proportion of deep-rooted vegetation in each cell (right panel Figure 4). f_{grass} is adjusted such that the total of all three HRUs is equal to 1 (i.e. $f_{grass} = 1 - [f_{imp} + f_{tree}]$, Vaze et al. 2018: Table 1). See section 1.4.3 for more details.

P_{refmap} Reference precipitation [mm/d] which controls infiltration-excess runoff further derived from slope β and $K_{0satPEDO}$ using an empirical relationship (see section 2.1.1). Figure 6 shows the final value used in AWRA-L v7 after scaling of the mapped value according to model parameter optimisation.

$K_{xsatPEDO}$ Saturated hydraulic conductivity [mm/d] for the top ($x=0$), shallow ($x=s$) and deep ($x=d$) layers defining the drainage rate when saturated (see section 2.1.2). These values were derived using pedotransfer functions based on clay content. Figure 7 shows the value used in AWRA-L v7 based on spatial maps (continental scale mapping of clay content from the Soil and Landscape Grids of Australia see: Vaze et al., 2018, Appendix A) and after scaling of the mapped values according to model parameter optimisation. The final values were derived using recent CSIRO digital soil mapping of Australian soil properties, specifically soil texture (sand, silt, clay and bulk density) and selected Pedotransfer functions to predict K_{sat} .

S_{xAWC} Available water storage fraction for top ($x=0$), shallow ($x=s$) and deep ($x=d$) layers (see section 2.1.2). These values were derived from the Soil and Landscape Grids of Australia as described in Vaze et al. (2018) with Figure 7 showing the value used in AWRA-L v7 based on spatial maps after scaling of the mapped values according to model parameter optimisation.

β Slope of the land surface [percent] derived according to Digital Elevation Model (DEM) analysis (Figure 8). Slope affects infiltration excess runoff (through Reference precipitation P_{ref} ; see section 2.1.1) and the proportion of drainage that occurs laterally as interflow (section 2.1.2).

K_{gmap} The groundwater drainage coefficient controls the baseflow rate – see section 2.1.3. Figure 9 shows the value used in AWRA-L v7 after

transforming the mapped values according to model parameter optimisation.

n_{map} Effective porosity affects lateral groundwater flow (baseflow; through K_{gmap}), along with the fraction saturated groundwater (which effects the amount of saturated overland flow) and the fraction of groundwater available for transpiration (Figure 10)

Hypsometric

curve The hypsometric curve is the cumulative distribution of elevation within an AWRA grid cell. This was derived based on a 3 sec SRTM DEM (Vaze et al. 2018: Table1; Peeters et al. 2013). This is used for conversion from groundwater storage to head relative to the lowest point in the cell. The head level determines the fraction saturated groundwater (which effects the amount of saturated overland flow) and fraction of groundwater available transpiration – see Figure 11 and section 2.1.3.

$\overline{E^*}$ Long term mean daily evapotranspiration is related by an empirical equation to the routing delay for streamflow (Figure 12)

U_{dMAX} Defines the deep soil maximum root water uptake rates. This value is calculated based on [Foliage Projective Cover \(FPC\) map](#) from the Landsat satellite (Gill et al. 2017); see Figure 13(a). Figure 13(b) shows the resulting U_{dMAX} value used in AWRA-L v7 (see section 1.4.3) following parameter optimisation. This value was set as a uniform value in previous versions of AWRA-L.

h_{veg} Vegetation height of deep-rooted vegetation (i.e., to the top of the canopy for tall vegetation and derived from lidar estimates) alters the aerodynamic conductance. Figure 14 shows the value used in AWRA-L v7 based on Vaze et al (2018).

LAI_{max} Maximum leaf area index defines the maximum achievable canopy cover in a particular cell (Figure 15).

The figures referenced above show the resulting parameters used in AWRA-L, often according to a transformation of scaling undertaken through the calibration process.

1.4.3 HRU proportions (f_{grass} , f_{imp} , f_{tree})

Each spatial unit (grid cell) in AWRA-L is divided into HRUs representing different landscape components. Hydrological processes, with the exception of groundwater storage, are modelled separately for each HRU before the resulting fluxes are combined to give cell outputs. The fluxes are combined using a weighted sum based on the proportion of each HRU. The current version of AWRA-L includes three HRUs which notionally represent (i) tall, deep-rooted vegetation (i.e. trees), (ii) short, shallow-

rooted vegetation (i.e. grass), and (iii) impervious landscapes (i.e. rock and urbanised area) with the root depth equal to zero.

Hydrologically, the HRUs differ in their aerodynamic control of evaporation, in their interception capacities and in their degree of access to different soil layers. Shallow rooted vegetation is distinguished from deep-rooted vegetation based on the Advanced Very High Resolution radiometer (AVHRR) satellite derived fractions of persistent and recurrent photosynthetically active absorbed radiation (fPAR) from 1992 to 2010 (Donohue, Roderick, and McVicar 2008). The persistent vegetation is interpreted to be tree cover (deep-rooted) and recurrent vegetation is interpreted to be grass cover (shallow rooted) (Figure 4).

An impervious surface HRU has been added to the existing shallow and deep-rooted vegetation HRUs in AWRA v7. The impervious HRU comprises urban landscapes and naturally impervious areas/rocky outcrops. This new HRU was derived by combining impervious area mapping from Geoscience Australia (dynamic landcover mapping product 2 for 2012-2013: urban class) and rocky-outcrop mapping derived from satellite vegetation using MODIS Enhanced Vegetation Index (EVI) covering the period 2000-2011 and terrain analysis (Juan Guerschman, CSIRO, pers comm.). Time series of EVI from MOD13Q1 (MODIS 16-day vegetation indices) at 250m resolution along with the Multiresolution Bottom Valley Index (Gallant and Dowling 2003) derived from the 1 second DEM of Australia were used to distinguish between rocky outcrops and sandy areas, in an Australia wide analysis to produce maps of permanently unvegetated areas.

For the impervious HRU water balance, if precipitation is greater than potential evaporation, actual evaporation is equal to potential evaporation and the remaining water is added to surface runoff. Otherwise actual evaporation is considered equal to precipitation and surface runoff is set to zero (Vaze et al., 2018). It has no infiltration into the soil profile and the canopy rainfall interception storage is zero because there is no vegetation on the impervious areas. The HRU fractions are assumed to remain static throughout the simulation, which mean they will overestimate impervious area for early simulations (eg. years prior to 2000) and underestimate future potential urban growth.

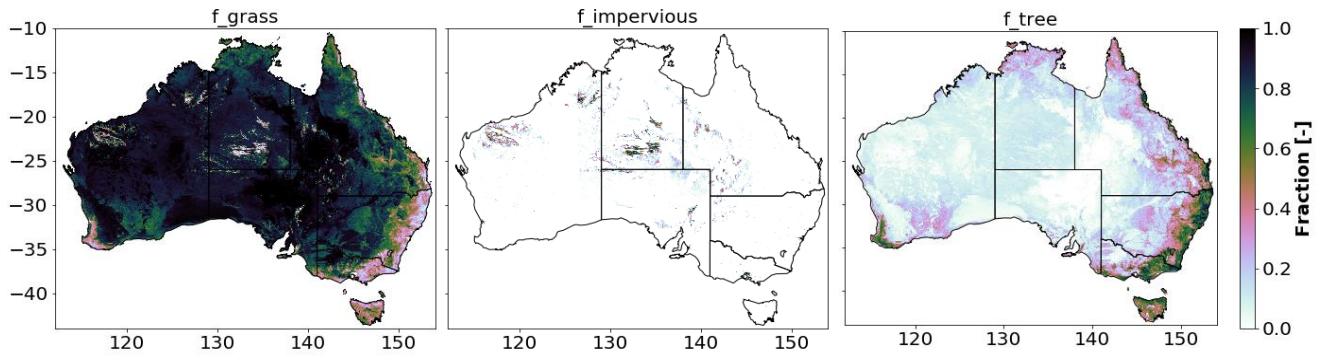


Figure 4. Fraction shallow-rooted, impervious, and deep-rooted areas within each grid cell

In reality the areas identified as impervious are partially impervious. To consider partial imperviousness due to the existence of green coverage and exposed soil within the urban landscapes along with outcrops in rocks, a scaling parameter was added to the model to address this issue. The scaling parameter (f_{imp_scale}) scales impervious area by a fraction [0-1] and re-attributes the remaining area to the shallow and deep rooted HRUs proportionally as follows:

$$f_{imp_scaled} = f_{imp} \times f_{imp_scale}$$

$$f_{tree_scaled} = f_{tree} + (1 - f_{imp} \times f_{imp_scale}) \times \left(\frac{f_{tree}}{f_{tree} + f_{grass}} \right)$$

$$f_{grass_scaled} = f_{grass} + (1 - f_{imp} \times f_{imp_scale}) \times \left(\frac{f_{grass}}{f_{tree} + f_{grass}} \right)$$

This approach was trialed over a set of impervious catchments and was shown to reduce overestimation of runoff when assessed over a series of 13 catchments with greater than 5% urban impervious area (see Frost et al, 2021) so was adopted here.

2 Water balance

Figure 5 shows a conceptual diagram of the water balance processes modelled in AWRA-L. These processes are described in the following sections.

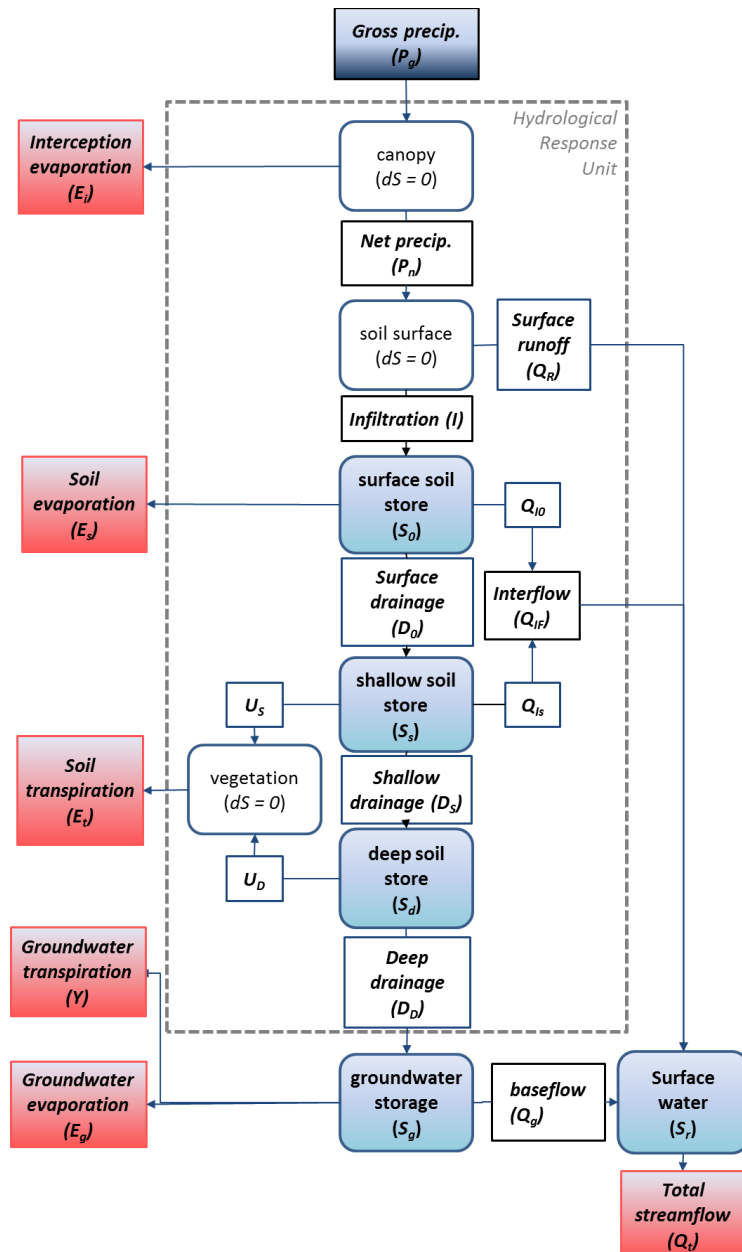


Figure 5. AWRA-L hydrological processes. Blue rounded boxes indicate water storages, white if no storage, white boxes are water balance fluxes, and red boxes are the output fluxes.

2.1 Water balance equations

The water balance in AWRA-L is represented by the following equations that partition the fluxes (ie. precipitation, infiltration, drainage, root water uptake, evaporation) into the modelled water stores (ie. top/shallow/deep soil, groundwater, surface water). All water storage and daily flux terms have millimetres [mm] for units. Throughout the document, (t) is used to denote the value corresponding to day t . All calculations below are undertaken for all HRUs separately, with the exception of the groundwater balance (considered as a single store) and total stream discharge (which are from a weighted sum of the flows over the three HRUs).

Gross rainfall (P_g) [mm] from the interpolated gridded daily input data after subtracting evaporation due to canopy interception (E_i), assuming no canopy storage, gives the net rainfall (P_n):

$$P_n(t) = \begin{cases} P_g(t) - E_i(t), & P_g > E_i \\ 0, & P_g \leq E_i \end{cases} \quad (1)$$

Soil surface partitioning of net rainfall into surface runoff (Q_R) and infiltration (I) gives:

$$I(t) = P_n(t) - Q_R(t) \quad (2)$$

Top layer soil water balance, comprising top layer soil water storage (S_0), infiltration, soil evaporation (E_s), interflow draining laterally from the top layer soil moisture (Q_{I0}) and top layer soil drainage (D_0):

$$S_0(t) = S_0(t-1) + I(t) - D_0(t) - Q_{I0}(t) - E_s(t) \quad (3)$$

Shallow soil water balance, comprising shallow soil water storage (S_s), shallow root water uptake (U_s), top layer soil drainage (D_0) from the layer above, interflow draining laterally from the shallow soil layer (Q_{Is}) and shallow soil water drainage (D_s):

$$S_s(t) = S_s(t-1) + D_0(t) - D_s(t) - Q_{Is}(t) - U_s(t) \quad (4)$$

Deep soil water balance, comprising deep soil water storage (S_d), D_s , deep root water uptake (U_d), and deep drainage (D_d):

$$S_d(t) = S_d(t-1) + D_s(t) - D_d(t) - U_d(t) \quad (5)$$

Groundwater balance, comprising ground water storage (S_g), D_d , root water uptake from groundwater store (Y), groundwater evaporation (E_g) and groundwater discharge (Q_g):

$$S_g(t) = S_g(t-1) + D_d(t) - Q_g(t) - E_g(t) - Y(t) \quad (6)$$

with each flux component a weighted sum according to the fraction HRU – denoted in bold here.

River water balance, comprising surface water storage (S_r), surface runoff (Q_R), interflow ($Q_I = Q_{I0} + Q_{Is}$), baseflow (Q_g), and total stream discharge (Q_t):

$$S_r(t) = S_r(t - 1) + Q_R(t) + Q_g(t) + Q_I(t) - Q_t(t) \quad (7)$$

2.1.1 Surface runoff ($Q_R = Q_h + Q_s$)

Gross rainfall following canopy interception evaporation (see section 3.3 for all vapour fluxes) gives net precipitation (P_n), which is further partitioned into surface runoff (Q_R) and infiltration (I) in eq (2).

Surface runoff ($Q_R = Q_h + Q_s$), is calculated as the sum of an infiltration-excess runoff component, Q_h , and a saturation-excess runoff component, Q_s .

All precipitation falling on the saturated fraction [-] of the landscape (f_{sat}) is assumed to run off, as saturation excess as per:

$$Q_s(t) = f_{sat}(t)P_n(t) \quad (8)$$

where calculation of the fraction of saturated area (f_{sat}) is dependent on the groundwater storage (S_g) relative to the topography as defined by the hypsometric curves – see section 2.1.3.

Infiltration-excess runoff is assumed to be generated from the unsaturated fraction ($1 - f_{sat}$) of the landscape at a rate that is modulated by the reference precipitation parameter P_{ref} :

$$Q_h(t) = (1 - f_{sat}(t)) \left(P_n(t) - P_{ref} \tanh \frac{P_n(t)}{P_{ref}} \right) \quad (9)$$

P_{ref} (Figure 6) represents the reference daily amount of the net precipitation that becomes infiltration excess runoff (N. Viney et al. 2015).

The original form of these equation was chosen by (Van Dijk, 2010b; Van Dijk, 2010c) and used a single value of P_{ref} spatially. Subsequent development introduced P_{ref} as an empirical function of the saturated hydraulic conductivity of surface soil ($K_{0satPEDO}$) and slope [percent] (β):

$$P_{ref} = P_{refscale} * P_{refmap} \quad (10)$$

where

$$P_{refmap} = 20 \left(2 + \log \left(\frac{K_{0satPEDO}}{\beta} \right) \right)$$

Following calculation of the surface runoff the infiltration component (I) is given by eq (2).

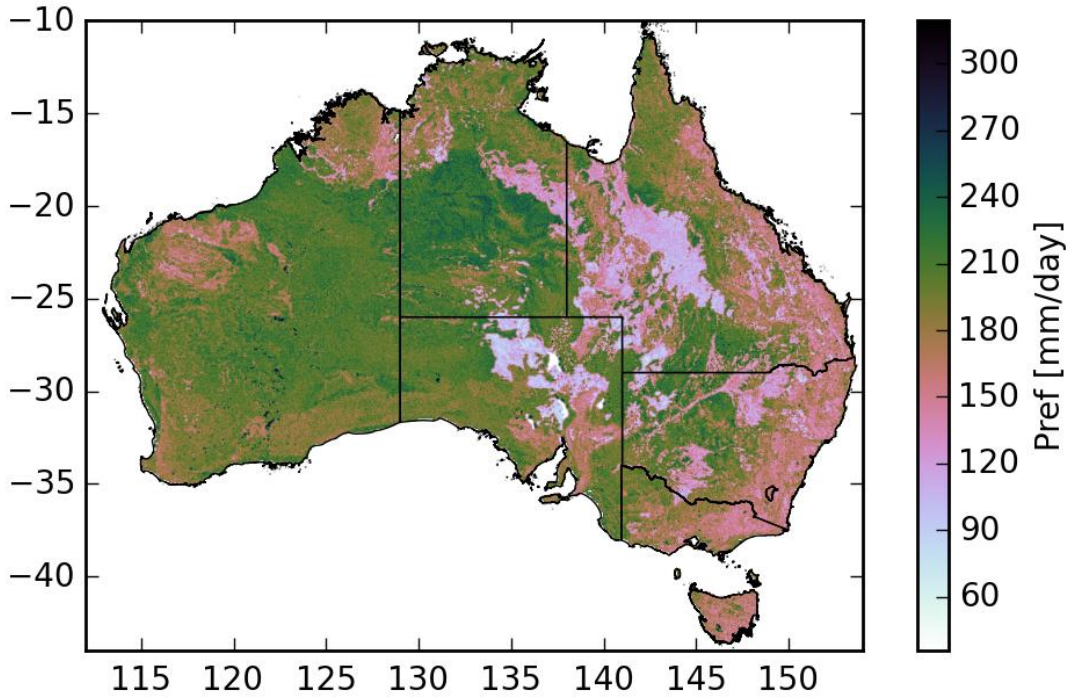


Figure 6. Continental distribution of reference precipitation (P_{ref}).

2.1.2 Soil storage (S_0, S_s, S_d), drainage (D_0, D_s, D_d) and interflow ($Q_{IF} = Q_{I0} + Q_{Is}$)

Total soil drainage (including vertical drainage and interflow) is assumed to occur according to the following equations for each soil layer.

For the top-soil layer drainage (D_0) and lateral interflow (Q_{I0}):

$$D_0(t) + Q_{I0}(t) = (K_{0sat}^m K_{ssat}^{1-m}) \left(\frac{S_0(t)}{S_{0max}} \right)^2 \quad (11)$$

Shallow soil layer drainage (D_s) and lateral interflow (Q_{Is}):

$$D_s(t) + Q_{Is}(t) = K_{ssat} \left(\frac{S_s(t)}{S_{smax}} \right)^2 \quad (12)$$

Deep soil layer drainage (D_d) assuming no lateral interflow from that layer:

$$D_d(t) = K_{dsat} \left(\frac{S_d(t)}{S_{dmax}} \right)^2 \quad (13)$$

Where $K_{x\text{sat}}$ and $S_{x\text{max}}$ represents the saturated hydraulic conductivity [mm/day] and maximum storage [mm] of the relevant soil layer x . In eq (11), m , is a weight parameter introduced in v7 for averaging the $K_{x\text{sat}}$ of the first two layers, towards better soil moisture and runoff performance. This equation was altered in v6 to increase the overall model performance, but that change sacrificed topsoil moisture accuracy. It revealed a trade-off between the accuracy of the estimates for the first two layers. In v7, a generalized alternative for eq (11) was used where a parameter, m , is introduced (that allows v5 through to v6 parameterisation, or any point in between. The values 1 and 0.5 set the equation to v6 and v5, respectively). The value for m was selected to be $\frac{2}{3}$ in v7 based on trials for the soil moisture validation data used in Frost et al (2021).

Total interflow (Q_{IF}) from the top and shallow soil layers is given by the sum:

$$Q_{IF} = Q_{I0} + Q_{Is} \quad (14)$$

The spatial maps of the parameters in equations 11-13 are shown in Figure 7. These drainage parameters are derived from the following equations:

$$S_{0\text{max}} = d_0 S_{0\text{AWC}} S_{0\text{maxscale}} \quad (15)$$

$$S_{s\text{max}} = d_s S_{s\text{AWC}} S_{s\text{maxscale}} \quad (16)$$

$$S_{d\text{max}} = d_d S_{d\text{AWC}} S_{d\text{maxscale}} \quad (17)$$

$$K_{0\text{sat}} = K_{0\text{satscale}} K_{0\text{satPEDO}} \quad (18)$$

$$K_{s\text{sat}} = K_{s\text{satscale}} K_{s\text{satPEDO}} \quad (19)$$

$$K_{d\text{sat}} = K_{d\text{satscale}} K_{d\text{satPEDO}} \quad (20)$$

Where d_0 , d_s and d_d are the depth of the top, shallow and deep soil layers (100mm, 900mm, 5000mm). $S_{0\text{AWC}}$, $S_{s\text{AWC}}$ and $S_{d\text{AWC}}$ are the (proportional) available water holding capacity of the top, shallow and deep layers. The plant available water capacity is the available water holding capacity divided by layer thickness). $K_{x\text{satPEDO}}$ is the saturated hydraulic conductivities of the relevant soil layers.

Available water capacities and saturated hydraulic conductivities are derived from pedotransfer functions applied to the continental scale mapping of clay content from the Soil and Landscape Grids of Australia (Vaze et al. 2018). The pedotransfer function of Dane and Puckett (1994) was used to estimate saturated conductivity ($K_{x\text{satPEDO}}$) for each layer:

$$K_{\text{satPEDO}} = 303.84 \exp(-0.144P_{<2}) \quad (21)$$

Where $P_{<2}$ is the clay fraction (i.e. $< 2 \mu\text{m}$ mass fraction of the $< 2 \text{mm}$ soil material determined using the pipette method). This pedotransfer function was recommended by Minasny and McBratney (2000) according to evaluation and comparison to other methods using Australian soil data.

Available water capacity was derived based on pedotransfer functions for soil water retention at field capacity (θ_{-33} : with -33kPa interpreted as the soil's capacity in the field to retain water) and wilting point (θ_{-1500} : with -1500kPa interpreted as the amount of water in the soil which will cause a plant to wilt):

$$S_{AWC} = \theta_{-33} - \theta_{-1500} \quad (22)$$

The following pedotransfer functions produced by Minasny *et al.* (1999) were used to estimate each of these components:

$$\theta_{-33} = 0.3543(1 - \exp(-0.0385P_{<2})) + 0.083 \quad (23)$$

$$\theta_{-1500} = 0.4016(1 - \exp(-0.0230P_{<2})) + 0.0027 \quad (24)$$

Further details of the approach for derivation of these spatial layers is described in Vaze *et al.* (2018).

The relative soil moisture w_x content of the soil layers (top, shallow and deep) is subsequently given by:

$$w_x(t) = \frac{S_x(t)}{S_{x\max}} \quad (25)$$

Where S_x is the soil storage and $S_{x\max}$ is the maximum storage for layer x .

Total drainage for each layer (defined by the right-hand side of equations (11-12) are partitioned into the drainage and interflow components (left hand side of equations 11-12) according to the following equations.

The proportion of overall top layer drainage that is lateral/interflow drainage (ρ_0) is given by:

$$\rho_0(t) = \tanh(k_\beta \beta \frac{S_0(t)}{S_{0\max}}) \tanh\left(k_\zeta \left(\frac{K_{0sat}}{K_{ssat}} - 1\right) \frac{S_0(t)}{S_{0\max}}\right) \quad (26)$$

The proportion of drainage that is lateral/interflow drainage for the shallow layer (ρ_s) is given by:

$$\rho_s(t) = \tanh(k_\beta \beta \frac{S_s(t)}{S_{s\max}}) \tanh\left(k_\zeta \left(\frac{K_{ssat}}{K_{dsat}} - 1\right) \frac{S_s(t)}{S_{s\max}}\right) \quad (27)$$

where β is the slope [radians] (noting radians are used here rather than percent elsewhere). Its values (see Figure 8) were derived by calculating average values from a 3 second DEM analysis (N. Viney *et al.* 2015). k_β is a dimensionless scaling factor and k_ζ is a scaling factor for the ratio of saturated hydraulic conductivity. The forms of the partitioning factor equations were chosen so that the proportion of drainage to interflow increases with increasing slope, soil moisture and the conductivity difference at the interface of the soil layers.

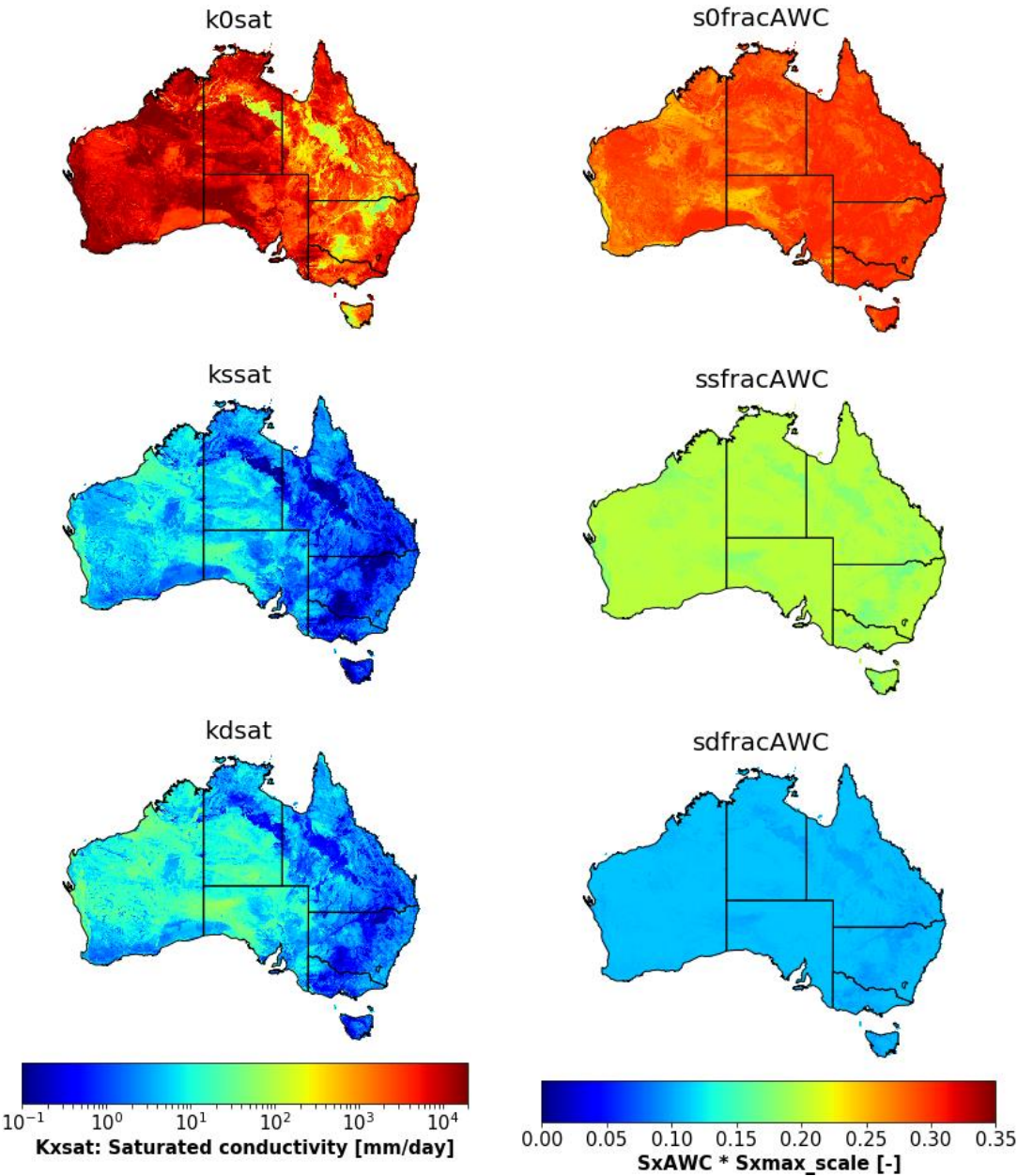


Figure 7. Saturated conductivity ($K_{x\text{sat}}$) and proportion available water capacity ($S_{s\text{AWC}}S_{s\text{maxscale}}$) for the top (0), shallow (s) and deep (d) soil layers.

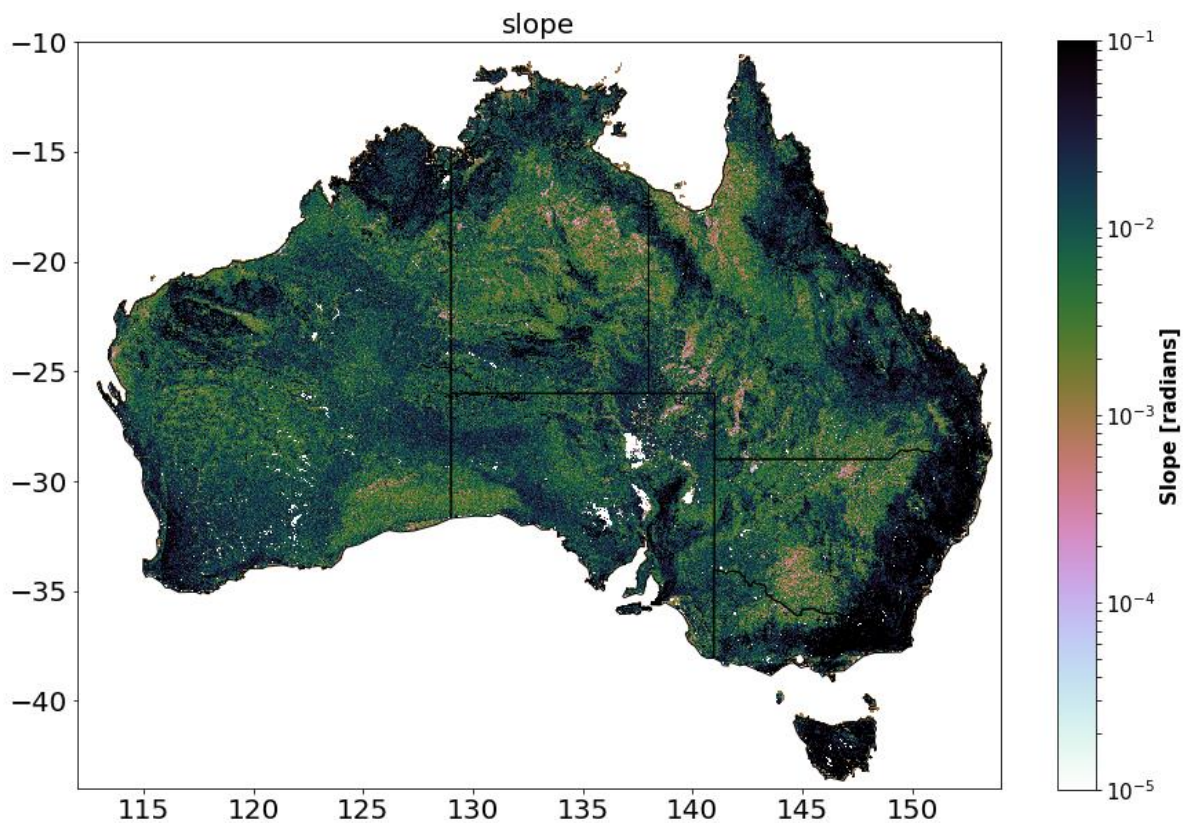


Figure 8. Average slope (β) within a grid from a 3 second DEM

2.1.3 Groundwater storage (S_g) and fluxes (Q_g, E_g, Y)

Groundwater balance (defined in eq. 6), comprises ground water storage (S_g), D_d , root water uptake from groundwater store (Y), groundwater evaporation (E_g) and groundwater discharge (Q_g).

Groundwater discharge to stream (baseflow) is conceptualised as a linear reservoir with the discharge being proportional to A_0 as a function of S_g according to:

$$Q_g(t) = A_0 * (1 - e^{-K_g S_g}) \quad (28)$$

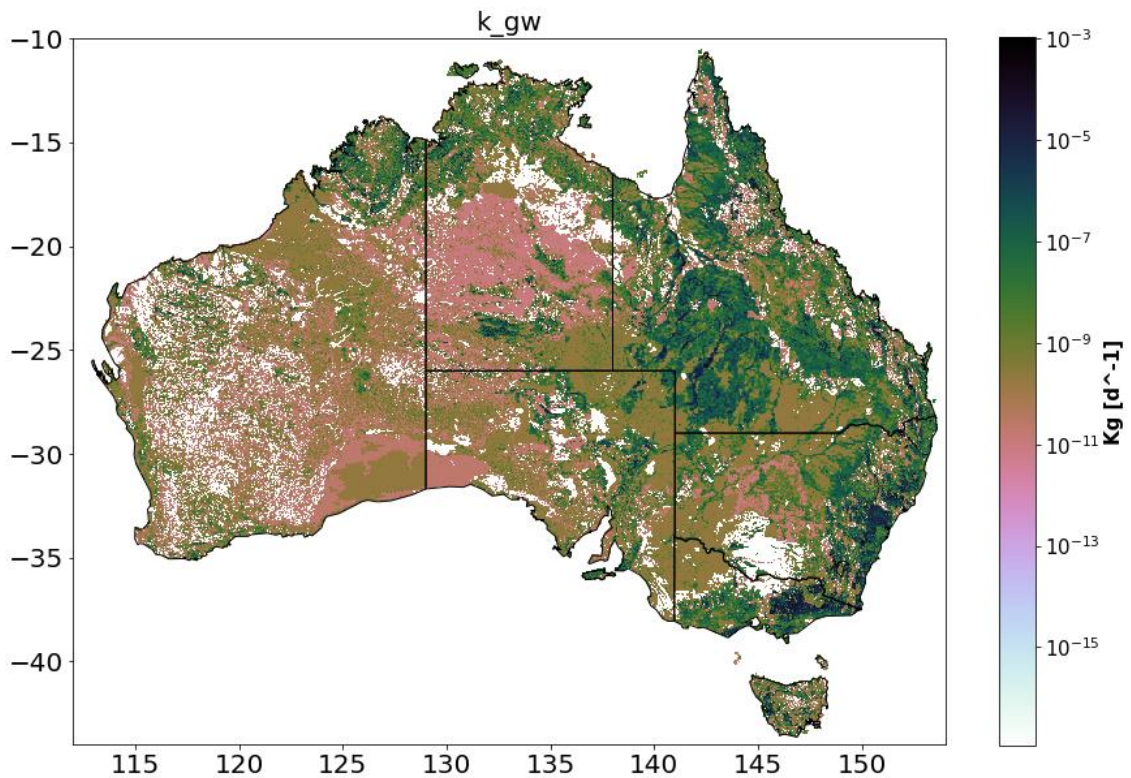


Figure 9. Groundwater drainage coefficient (K_g)

Where A_0 and K_g are the groundwater availability factor and groundwater drainage coefficient respectively. The formulation chosen here (eq 28), from analysis presented in Van Dijk, 2010a) is known as a linear reservoir equation and is commonly used in lumped catchment rainfall-runoff models (Van Dijk, 2010c). The groundwater availability factor is introduced in AWRA-L v7 (to replace directly using S_g) as a threshold mechanism to control baseflow discharge more closely (allowing baseflow cut-off at groundwater levels above the lowest point in the grid cell according to the hypsometric curve i.e. $S_g > 0$). This allows ephemerality of streamflow to be observed in Australia more easily, while not necessarily causing depletion of groundwater. In addition to the threshold, a Sigmoid function is introduced, so that the thresholding of baseflow is not all or nothing but ramps smoothly according to:

$$A_0 = \max \left(\left(\frac{2}{1 - e^{-\frac{S_g(t-1) + D_d(t) - \xi_0}{\mu_0}}} - 1 \right), 0 \right) \quad (29)$$

Where ξ_0 and μ_0 are the groundwater availability threshold and shape factors, respectively, both optimised through calibration. Baseflow only occurs when the storage level (nominally $S_g(t-1) + D_d(t)$ for the next timestep) exceeds the threshold level ξ_0 and stands above the drainage base H_b plus the threshold value (in eq 29). H_b [m] is the lowest topographic point within the grid cell (see section on hypsometric curves)

$$K_g = K_{g\text{scale}}(K_{g\text{map}}^{K_{g\text{power}}}) \quad (30)$$

$K_{g\text{map}}$ is the groundwater drainage coefficient obtained from continental mapping and $K_{g\text{scale}}$ and $K_{g\text{power}}$ are optimised factors. $K_{g\text{power}}$ is introduced in v7 to allow more or less contrasting (in terms of scales of K_g) than was previously available through the derived mapping of $K_{g\text{map}}$. This is derived from the depth to the unconfined aquifer (d_u), the elevation change along the flow path (h_u), and from continental mapping of surface water drainage density (λ_d) (not shown), and the effective porosity (n_{map}):

$$K_{g\text{map}} = \frac{k_u(2\lambda_d)^2 \max\{d_u, h_u\}}{n_{\text{map}}} \quad (31)$$

Groundwater evaporation and transpiration are dependent on the fraction of the grid cell that is saturated at the surface (f_{sat}) and the fraction of the grid cell that is accessible for transpiration (f_{Eg}). Both of these values are functions of the groundwater head (h) relative to the cumulative distribution of topography (termed hypsometric curves) within the cell (Peeters et al. 2013). In AWRA-L v7, distribution is based on a 3 sec SRTM based DEM (see Vaze et al. 2018: Table 1).

Groundwater storage (S_g) in mm is converted to head (in metres) according to:

$$S_g(t) = 1000nh(t) \quad (32)$$

Effective porosity (n) [-] is given by:

$$n = n_{\text{scale}} n_{\text{map}} \quad (33)$$

where n_{map} is effective porosity obtained from continental mapping and n_{scale} is the scaling factor for effective porosity.

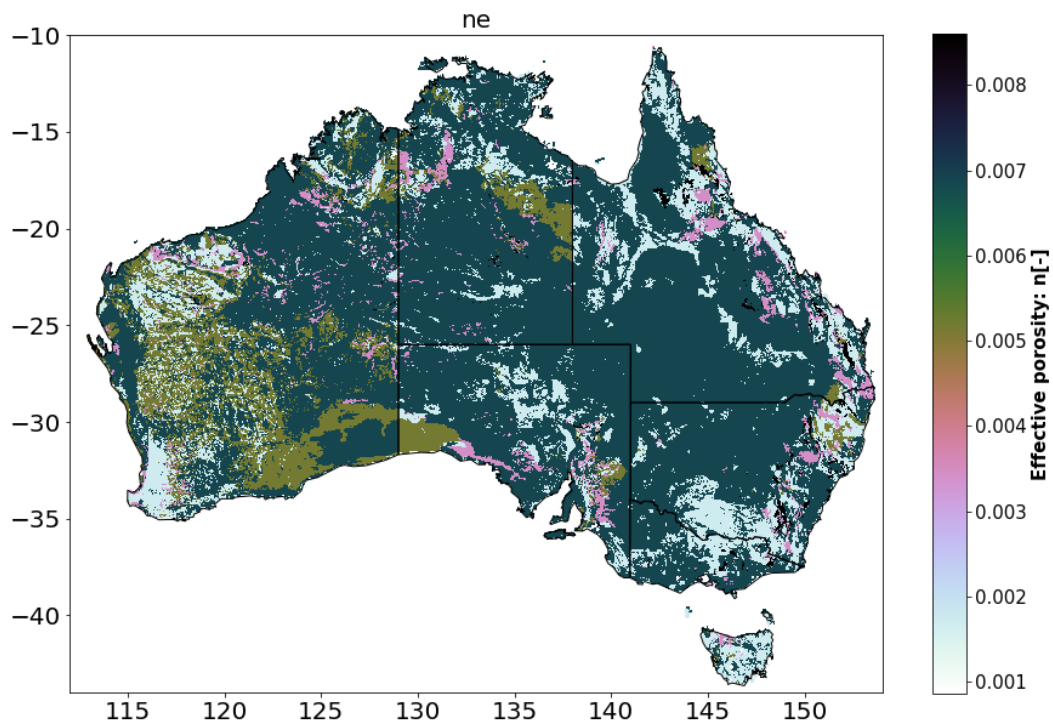


Figure 10. Effective porosity (n)

The fraction of the grid cell where the water table is above the ground surface is considered to be the saturated area. Thus, f_{sat} [-] is taken as the fraction on the cumulative curve at which elevation is equal to $1000nH_b + S_g$.

Similarly, the fraction of a grid cell that is accessible for the vegetation to transpire groundwater (f_{Eg}) is calculated as the fraction of the grid cell where the water table is above a plane of the rooting depth. That is, where the elevation is equal to $1000n(H_b + D_R) + S_g$, where D_R is the rooting depth [m]: currently set to the depth of the base deep-rooted vegetation within the deep soil store (6m).

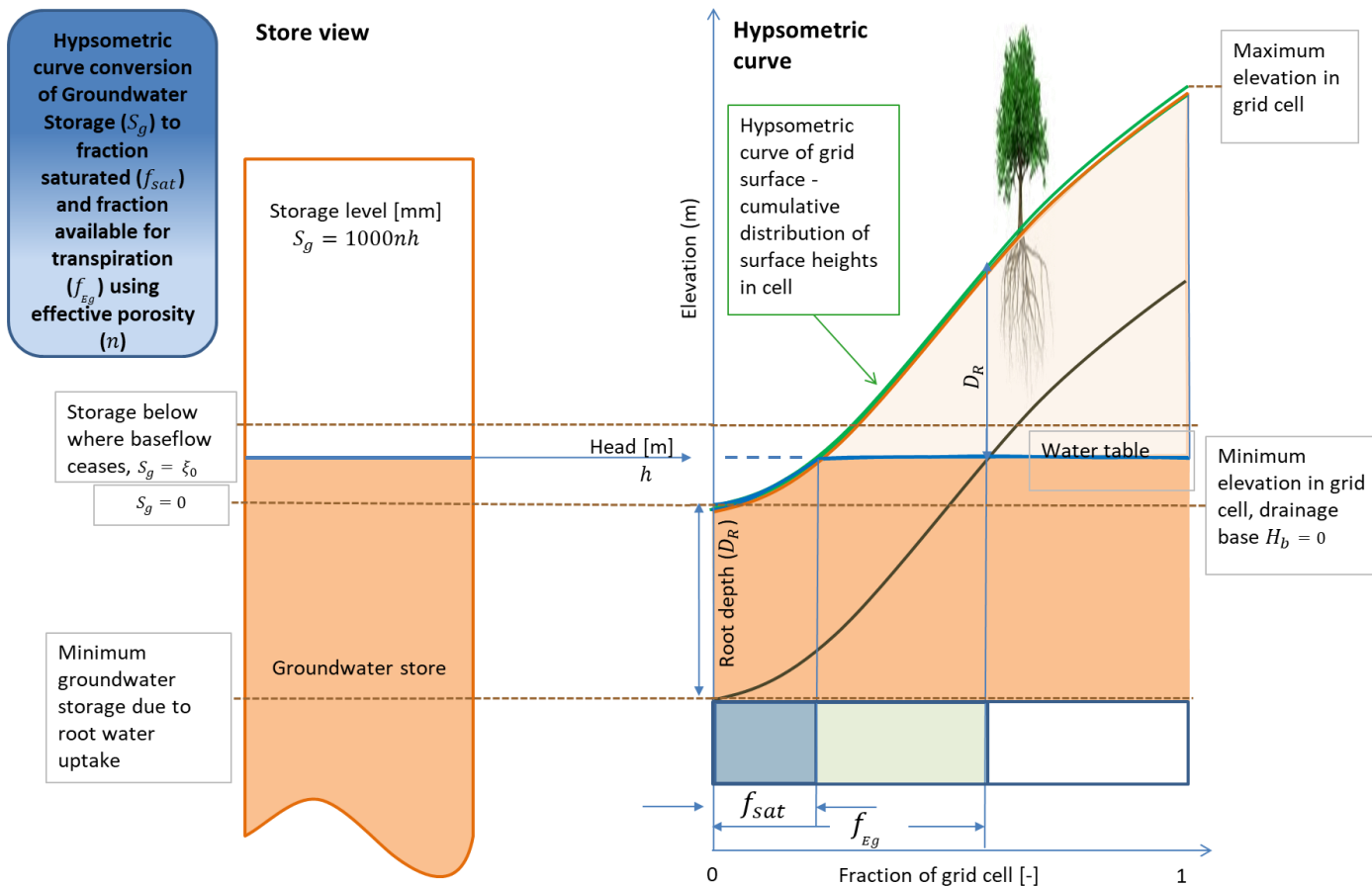


Figure 11. Hypsometric curve conversion of groundwater storage to fraction of cell saturated and fraction of cell available for transpiration

2.1.4 Total Streamflow and surface water storage

In AWRA-L, discharge (Q_t) is sourced from surface runoff, baseflow and interflow according to eq (7). Discharge of water from these sources is routed via a notional surface water store, S_r (mm). The purpose of this store is primarily to reproduce the partially delayed drainage of storm flow that is normally observed in all but the smallest and fastest responding catchments.

The discharge from this surface water store is controlled by a routing delay factor (K_r) according to:

$$Q_t(t) = (1 - e^{K_r}) (S_r(t - 1) + Q_h(t) + Q_s(t) + Q_g(t) + Q_l(t)) \quad (34)$$

Where the routing delay is calculated via a linear relationship with long term mean daily evapotranspiration ($\overline{E^*}$)

$$K_r = K_{rint} + K_{rscale} \overline{E^*} \quad (35)$$

where K_{rint} is an Intercept coefficient and K_{rscale} is a scale coefficient for calculating K_r . This relationship was chosen based on empirical analysis over 260 Australian catchments presented in Van Dijk (2010c, 2010b). It is noted that the two parameters in eq (35) are optimised.

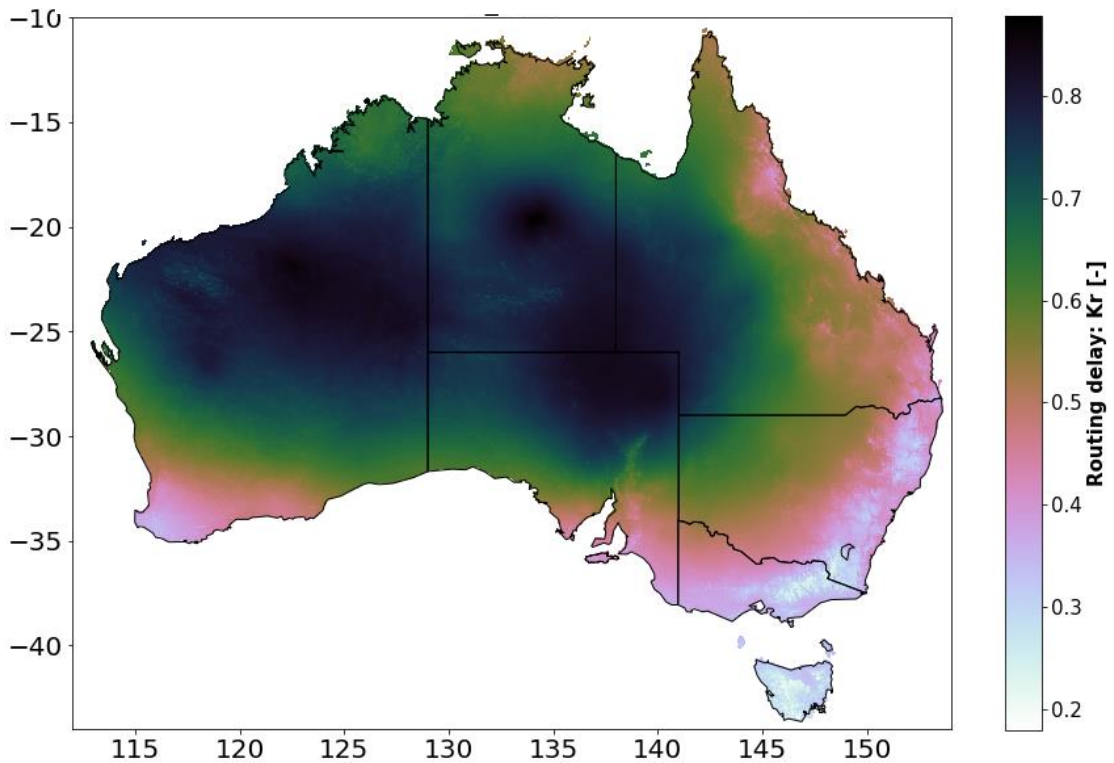


Figure 12. Streamflow routing coefficient (K_r)

3 Vapour fluxes and the energy balance

3.1 Potential evaporation (E_0)

An estimate of potential evaporation is a key element of the landscape modelling in AWRA-L. Potential evaporation is required to scale, and to provide an upper limit on, evaporation and transpiration processes from the soil and vegetation (see section 3.3).

Potential evaporation E_0 [mm/day] is calculated according to the Penman (1948) equation (N. Viney et al. 2015) as a combination of net radiation (the energy required to sustain evaporation) and vapour pressure deficit (multiplied by a wind function)

$$E_0(t) = \max \left\{ 0, \frac{\Delta(t)R_n(t) + 6.43\gamma[p_{es}(t) - p_e(t)][1 + 0.546u_2(t)]}{\lambda(t)[\Delta(t) + \gamma]} \right\} \quad (36)$$

where Δ [Pa/K] is the slope of the saturation vapour pressure curve, R_n [MJ m⁻² d⁻¹] net radiation, γ [Pa/K] the psychrometric constant, λ [MJ/kg] the latent heat of vaporisation, u_2 is wind speed at a height of 2 m [m/s], p_{es} [Pa] is saturation vapour pressure and p_e is actual vapour pressure [Pa].

Since eq (36) is intended to be applied at a daily time step, the soil heat flux is assumed to be negligible in comparison with the net radiation flux and is therefore ignored.

The latent heat of vaporisation λ is given by Shuttleworth (1992) and Allen *et al.* (1998) as:

$$\lambda(t) = 2.501 - 0.002361T_a(t) \quad (37)$$

where T_a [°C] is daily mean temperature, which was previously in AWRA-L v6 taken to be the weighted mean of the daily maximum (T_{max}) and minimum (T_{min}) temperatures with the weights, τ_{max} and $1 - \tau_{max}$ equal to 0.75 and 0.25 respectively (Raupach *et al.*, 2008)). This parameter was previously fixed, however has been released in calibration for v7 based on improved performance. τ_{max} and $1 - \tau_{max}$ were optimized respectively to 0.85 and 0.15 in v7.

$$T_a(t) = \begin{cases} \tau_{max}T_{max}(t) + (1 - \tau_{max})T_{min}(t) & \text{if } T_{min}(t) \leq T_{max}(t) \\ T_{max}(t) & \text{if } T_{min}(t) > T_{max}(t) \end{cases} \quad (38)$$

As Van Dijk (2010a) notes, several of the temperature-dependent functions used are strongly non-linear and therefore the above approximation will possibly introduce error, although its magnitude is unknown.

The slope of the saturation vapour pressure curve is:

$$\Delta(t) = 4217.457 \frac{p_{es}(t)}{(240.97 + T_a(t))^2} \quad (39)$$

Saturation vapour pressure (p_{es}) is given according to the following approximation (Shuttleworth 1992):

$$p_{es}(t) = 610.8 \exp\left(\frac{17.27T_a(t)}{237.3 + T_a(t)}\right) \quad (40)$$

3.2 The energy balance

Potential evaporation depends on the available energy at the surface, which is given by the net radiation term (R_n) [MJ/m²/day]. This term, in turn, requires estimation of its constituent upward and downward fluxes of shortwave and longwave radiation:

$$R_n(t) = K_d(t) - K_u(t) + L_d(t) - L_u(t) \quad (41)$$

where K_d is downward (incoming) solar radiation, K_u the reflected outgoing shortwave radiation, L_d the cloud reflected downward (incoming) longwave radiation and L_u the outgoing terrestrial radiation. As E_0 is intended to apply at a daily time step, the soil heat flux is assumed to be negligible in comparison with the net radiation flux, and is therefore ignored.

3.2.1 Upward and Downward shortwave radiation

Downward shortwave radiation K_d [MJ/m²/day] is given according to the gridded input solar radiation data (section 1.4.1). The upward shortwave radiation K_u [MJ/m²/day] is calculated from K_d and the land surface albedo α [-]:

$$K_u(t) = \alpha(t)K_d(t) \quad (42)$$

where

$$\alpha(t) = f_v(t)\alpha_v + f_s(t)\alpha_s(t) \quad (43)$$

with f_v [-] the fractional canopy cover, α_v [-] the vegetation albedo, f_s [-] is the fraction of soil cover, and α_s [-] the soil albedo.

Fractional canopy cover f_v estimation is discussed in Section 4 (Vegetation Phenology). The fraction of soil cover is the portion that is not living vegetation and includes soil, rock, dead biomass and other land cover:

$$f_s(t) = 1 - f_v(t) \quad (44)$$

The vegetation albedo α_v [-] is calculated from the vegetation photosynthetic capacity index (per unit canopy cover) V_c [-] as:

$$\alpha_v = 0.452V_c \quad (45)$$

The relationship was derived using MODIS broadband white sky albedo. The photosynthetic capacity index V_c was calculated from MODIS Enhanced Vegetation Index, with MODIS fPAR used to estimate the fractional canopy cover f_v . In v6 and previous versions V_c was fixed to 0.65 and 0.35 for shallow and deep-rooted vegetation (respectively) – see Van Dijk (2010c). They are updated in AWRA-L v7 (according to manual experimentation) to match the modelled albedo with MODIS albedo observation to 0.26 and 0.18.

The soil albedo α_s [-] is calculated from the wet soil albedo α_{wet} [-] and the dry soil albedo α_{dry} [-]

$$\alpha_s(t) = \alpha_{wet} + (\alpha_{dry} - \alpha_{wet}) e^{-\left(\frac{w_0(t)}{w_{0ref}}\right)} \quad (46)$$

where the relationship between albedo and surface soil moisture was derived using MODIS broadband white sky albedo and ASAR surface soil moisture. In AWRA-L v7, the parameters of α_s as wet soil albedo α_{wet} and dry soil albedo α_{dry} are fixed (tuned manually to match albedo dynamics) to 0.08 and 0.18, and the reference value of w_{0ref} (determining the rate of albedo decrease with wetness) is fixed to 0.85 (following Van Dijk, 2010c).

3.2.2 Upward longwave radiation

Upward longwave radiation L_u [W/m²] is calculated according to black body theory with the terrestrial surface radiation given as $\varepsilon\sigma T^4$. Assuming a surface emissivity ε of 1 (Van Dijk, 2010c) and using the air temperature T_a [°C] as an estimate of the surface temperature [°K] gives

$$L_u(t) = \sigma(T_a(t) + 273.15)^4 \quad (47)$$

with σ [W/m²/K⁴] the Stefan-Boltzmann constant represented as 5.67×10^{-8} in the model (Dong *et al.*, 1992; Donohue, McVicar and Roderick, 2009).

3.2.3 Downward longwave radiation

The downward longwave radiation L_d [W/m²] is calculated from:

$$L_d(t) = \sigma(T_a(t) + 273.15)^4 \left\{ 1 - \left[1 - 0.65 \left(\frac{e_a(t)}{T_a(t) + 273.15} \right)^{0.14} \right] \left(1.35 \frac{K_{d0}(t)}{K_{d0}(DOY)} - 0.35 \right) \right\} \quad (48)$$

Where K_{d0} is the expected downwelling shortwave radiation on a cloudless day (MJ m⁻² d⁻¹) as a function of the numeric day of the year (DOY), latitude (ϕ) [radians], solar declination δ [radians] and ω the sunset hour angle [radians]:

$$K_{d0}(DOY) = \frac{94.5 \left(1 + 0.033 \cos\left(\frac{2\pi DOY}{365}\right) \right)}{\pi} (\omega \sin \delta \sin \phi + \cos \delta \cos \phi \sin \omega) \quad (49)$$

$$\delta = 0.006918 - 0.39912 \cos(Q_0) + 0.070257 \sin(Q_0) - 0.006758 \cos(2Q_0) + 0.000907 \sin(2Q_0) - 0.002697 \cos(3Q_0) + 0.00148 \sin(3Q_0) \quad (50)$$

$$Q_0 = \frac{2\pi(DOY-1)}{365} \quad (51)$$

This is similar to the equation for L_d in Donohue *et al.* (2009), but with different parameterisations for the atmospheric emissivity and transmissivity for a clear sky. It is noted that this is different from the initial derivation provided by Van Dijk (2010c), as

downwelling longwave radiation is now augmented by radiation from the cloud base (see Viney et al, 2015). The derivation is detailed in Appendix B.

3.3 Actual evapotranspiration (E_{tot})

Total actual evapotranspiration E_{tot} [mm] is the sum of evaporation (interception E_i , soil E_s and groundwater E_g) and transpiration (shallow U_s and deep U_d root water uptake, transpiration from groundwater Y):

$$E_{tot} = E_i + E_s + E_g + U_s + U_d + Y \quad (52)$$

each described below. It is noted that Canopy interception and transpiration from groundwater are not limited by the total sum being less than potential evaporation – hence total values greater than potential can occur on a given day. This approach was introduced by van Dijk (2010) in AWRA-L v0.5 as several mechanisms have been proposed that would effectively increase available energy to beyond potential evaporation, for this reason, estimated interception evaporation is not subjected to the energy constraint of E_{tot} , nor is available energy for the remaining evaporation fluxes (occurring during dry periods) reduced. Because the physics of rainfall interception are not well understood, it is also as yet unclear to what extent wet canopy evaporation rates are influenced by canopy cover and density (VanDijk 2010).

3.3.1 Interception evaporation (E_i)

The evaporation of intercepted rainfall (E_i), following VanDijk (2010), is the widely adopted and evaluated event-based rainfall interception model of Gash (1979), with modifications made later by Gash, Lloyd and Lachaudb (1995) and Van Dijk and Bruijnzeel (2001) to allow application to vegetation with a sparse canopy.

$$E_i(t) = \begin{cases} f_v(t)P_g(t) & \text{if } P_g(t) < P_{wet}(t) \\ f_v(t)P_{wet}(t) + f_{ER}(t)(P_g(t) - P_{wet}(t)) & \text{if } P_g(t) \geq P_{wet}(t) \end{cases} \quad (53)$$

where f_v [-] is the fractional canopy cover (see Section 4 Vegetation Phenology), P_{wet} [mm] is the reference threshold rainfall amount at which the canopy is wet:

$$P_{wet}(t) = -\ln\left(1 - \frac{f_{ER}(t)}{f_v(t)} \frac{S_{veg}(t)}{f_{ER}(t)}\right) \quad (54)$$

For small rainfall events where $P_g(t) < P_{wet}(t)$, all rainfall that falls on the vegetated part of the landscape is assumed to be intercepted. The energy required for evaporation of intercepted water is assumed independent of potential evaporation. It is further assumed that this energy does not reduce the available energy for the remaining evaporative fluxes.

The canopy rainfall storage capacity S_{veg} [mm] given by

$$S_{veg}(t) = s_{leaf} LAI(t) \quad (55)$$

where the specific canopy rainfall storage capacity per unit leaf area s_{leaf} [mm] is a HRU specific calibration parameter. LAI is the Leaf Area Index [-], the one-sided green leaf area per unit ground surface area, that is directly related to f_v (see Section 4).

The ratio of average evaporation rate to average rainfall intensity (during storms) f_{ER} [-] is:

$$f_{ER}(t) = F_{ER0} f_v(t) \quad (56)$$

where the specific ratio of average evaporation rate over average rainfall intensity during storms per unit canopy cover F_{ER0} [-] is a calibration parameter.

3.3.2 Soil evaporation (E_s)

The evaporation from soil E_s [mm] occurs from the unsaturated portion of the grid cell ($1 - f_{sat}$), as a fraction of the potential evaporation (E_0) possible after shallow and deep (E_t) rooted transpiration (described below) have been subtracted:

$$E_s(t) = (1 - f_{sat}(t)) f_{soil E}(t) [E_0(t) - E_t(t)] \quad (57)$$

where the relative soil evaporation $f_{soil E}$ [-] is

$$f_{soil E}(t) = f_{soil E max} \min\left(1, \frac{w_0(t)}{w_{0lim E}}\right) \quad (58)$$

and $f_{soil E max}$ is the relative soil evaporation when soil water supply is not limiting and $w_{0lim E}$ [-] is the relative top layer soil moisture at which evaporation is reduced.

3.3.3 Evaporation from groundwater (E_g)

The evaporation from groundwater E_g [mm/day] occurs from the saturated portion of the grid cell (f_{sat}), as a fraction of the potential evaporation (E_0) possible after shallow and deep (E_t) rooted transpiration (described below) have been subtracted:

$$E_g(t) = f_{sat}(t) f_{soil E max} [E_0(t) - E_t(t)] \quad (59)$$

where the same model as the evaporation from soil is used, with the top soil layer saturated ($w_0(t) = 1$).

3.3.4 Root water uptake from ($E_t = U_s + U_d$)

Total transpiration from plants E_t [mm] in the shallow and deep soil stores is equivalent to the sum of root water uptake from the shallow and deep-rooted vegetation. The transpiration fluxes are limited by two factors: a potential transpiration rate $E_{t max}$ and a maximum root water uptake U_0 . The actual transpiration is then calculated as the lesser of the two and this amount is distributed among the potential transpiration water

sources. The overall transpiration rate given by U is used in the estimation of U_s and U_d , the shallow and deep-rooted vegetation transpiration respectively. As U_s and U_d may be limited by available soil water, an adjusted total transpiration rate is finally recalculated. This final value of E_t is then used to reduce the energy available for direct evaporation.

The maximum root water uptake under ambient conditions U_0 [mm/day] is simply the greater of the maximum root water uptake from the shallow soil store $U_{s\ max}$ [mm/day] and the deep soil store $U_{d\ max}$ [mm/day]:

$$U_0(t) = \max[U_{s\ max}(t), U_{d\ max}(t)] \quad (60)$$

with the maximum root water uptake from the shallow soil store $U_{s\ max}$ [mm/day] given by:

$$U_{s\ max}(t) = U_{s\ MAX} \min\left(1, \frac{w_s(t)}{w_{s\ lim}}\right) \quad (61)$$

with the physiological maximum root water uptake from the shallow soil store $U_{s\ MAX}$ [mm/day] a parameter that is fixed to 6 for both the deep and shallow rooted HRU based on site water use at flux towers (Van Dijk, 2010c). Similarly, the relative shallow soil water content at which transpiration is reduced $w_{s\ lim}$ is fixed to 0.3 for both deep and shallow HRUs.

The maximum root water uptake from the deep soil store $U_{d\ max}$ [mm/day] is given by

$$U_{d\ max}(t) = U_{d\ MAX} \min\left(1, \frac{w_d(t)}{w_{d\ lim}}\right) \quad (62)$$

with the physiological maximum root water uptake from the deep soil store $U_{d\ MAX}$ [mm/day] and fixed to 0 for the shallow rooted HRU. The $U_{d\ MAX}$ was a single calibrated parameter in v6. However, $U_{d\ MAX}$ is in reality spatially variable depending on vegetation density. Therefore, to improve the model ET accuracy, the single continental value was replaced with a spatially varying static map in v7 (Figure 13). According to Kelley et al. (2007), water use of trees can be represented as a linear function of Tree Basal Area (TBA: [m²/ha]):

$$U_{d\ MAX} = MTTPT \times TBA \quad (63)$$

It is noted that this relationship was derived from averages of water use observed in the Australian wet season, and therefore the relationship holds for periods of high radiation load and high soil water content. This approach follows that adopted by Owens et al (2019) for a similar biophysical model GRASP. TBA can be calculated following the relationship developed by Armston et al. (2009):

$$TBA = \frac{-38.6 \log(1-FPC)}{1-0.36 \log(1-FPC)} \quad (64)$$

where FPC is the foliage projected cover (<http://data.auscover.org.au/xwiki/bin/view/Product+pages/Persistent+Green-Vegetation+Fraction>, Gill et al., 2017)

For the relative deep soil water content at which transpiration is reduced $w_{d\ lim}$, the value is fixed to 0.3 for both deep and shallow HRUs.

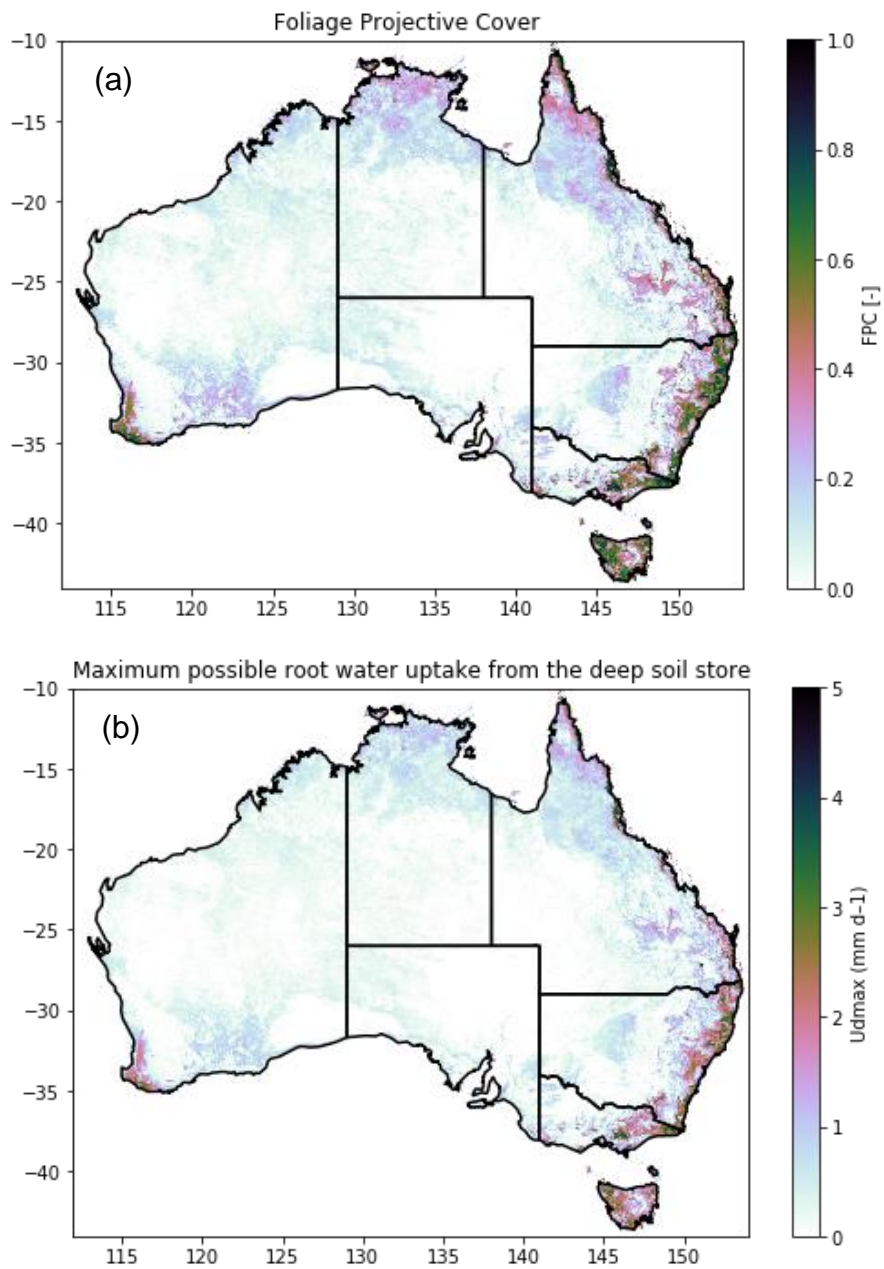


Figure 13. (a) Foliage Projective Cover (FPC) and (b) Maximum possible root water uptake from the deep soil store (U_{dMAX})

The root water uptake U [mm/day] is simply the lesser of the maximum root water uptake under ambient conditions U_0 [mm/day] and the maximum transpiration $E_{t\ max}$ [mm/day]

$$U(t) = \min[U_0(t), E_{t\ max}(t)] \quad (65)$$

where the maximum transpiration $E_{t\ max}$ [mm/day] is given by

$$E_{t\ max}(t) = f_t(t)E_0(t) \quad (66)$$

and the potential transpiration fraction f_t [-] is given by

$$f_t(t) = \frac{1}{1 + \left(\frac{k_\varepsilon(t)}{1 + k_\varepsilon(t)}\right) \frac{g_a(t)}{g_s(t)}} \quad (67)$$

Where g_a [m/s] is aerodynamic conductance, and g_s [m/s] the canopy conductance, and k_ε [-] is a coefficient that determines evaporation efficiency:

$$k_\varepsilon(t) = \Delta(t)/\gamma \quad (68)$$

where Δ [Pa/K] is the slope of the saturation vapour pressure curve, R_n [$\text{MJ m}^{-2} \text{d}^{-1}$] net radiation, γ [Pa/K] the psychrometric constant.

Aerodynamic conductance (g_a) is given by:

$$g_a(t) = \frac{0.305 u_2(t)}{\ln\left(\frac{813}{h_{veg}} - 5.45\right) \left(2.3 + \ln\left(\frac{813}{h_{veg}} - 5.45\right)\right)} \quad (69)$$

where h_{veg} is the height of the vegetation canopy [m]. This equation was derived by Van Dijk (2010a) based on the well-established theory proposed by Thom (1975). The derivation is provided in Appendix B.

The height of the top of the canopy (Figure 14) is derived from the global 1 km Lidar estimates of Simard *et al.* (2011) and is assumed to be appropriate only for the deep-rooted HRU. For the shallow-rooted HRU, the vegetation height is parameter and is assumed to take a fixed value of 0.5 m in AWRA-L v7. Vegetation height is assumed static throughout the simulation.

Canopy (surface) conductance g_s [m/s] is given by:

$$g_s(t) = f_v(t)c_{g_s\ max}V_c \quad (70)$$

where f_v the fractional canopy cover is discussed in Section 4, $c_{g_s\ max}$ is a coefficient relating vegetation photosynthetic capacity to maximum stomatal conductance (m s^{-1}), and V_c is vegetation photosynthetic capacity index (per unit canopy cover) described in section 3.2 (Energy Balance). $c_{g_s\ max}$ is currently optimised for both the shallow and deep-rooted HRUs, although Van Dijk (2010a) showed that an a priori estimate of 0.03 may be justified.

The root water uptake from the shallow soil store U_s [mm/day] is given by:

$$U_s(t) = \begin{cases} \min \left[S_s(t) - 0.01, \left(\frac{U_s \max(t)}{U_s \max(t) + U_d \max(t)} \right) U(t) \right] & \text{if } U_0(t) > 0 \\ 0 & \text{if } U_0(t) \leq 0 \end{cases} \quad (71)$$

The root water uptake from the deep soil store U_d [mm/day] is given by:

$$U_d(t) = \begin{cases} \min \left[S_d(t) - 0.01, \left(\frac{U_d \max(t)}{U_s \max(t) + U_d \max(t)} \right) U(t) \right] & \text{if } U_0(t) > 0 \\ 0 & \text{if } U_0(t) \leq 0 \end{cases} \quad (72)$$

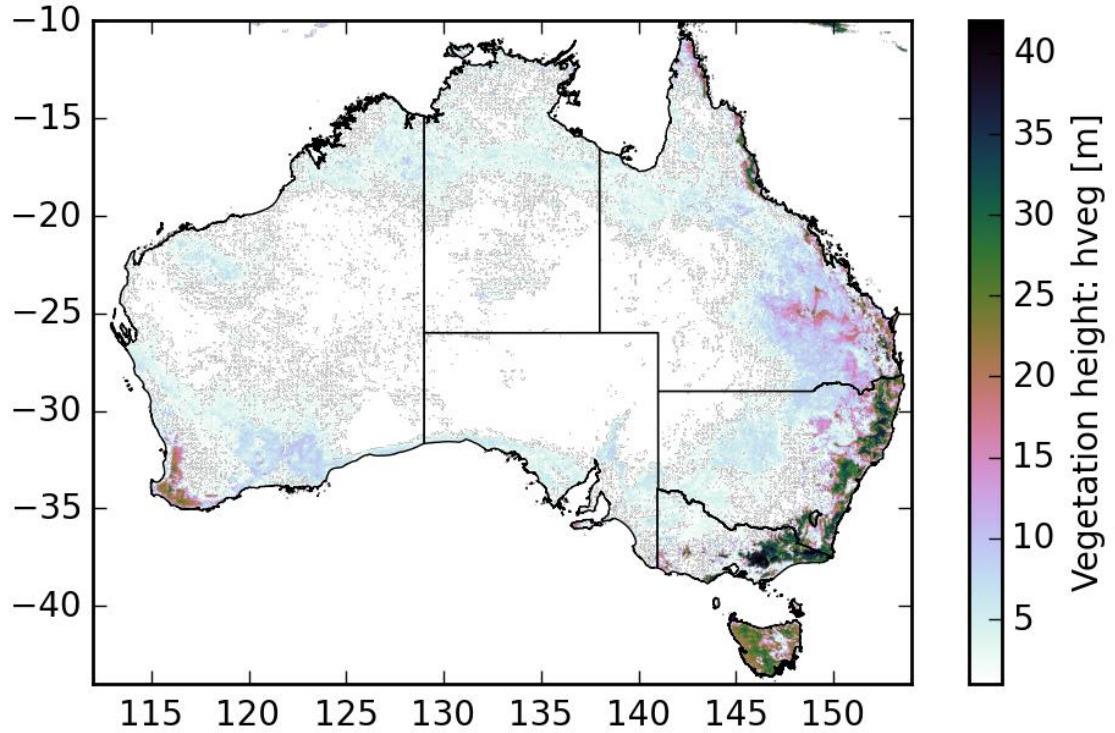


Figure 14. Vegetation height of deep-rooted vegetation (h_{veg})

3.3.5 Transpiration from groundwater (Y)

Transpiration from the groundwater store (Y) [mm/day] is given by

$$Y(t) = \begin{cases} \left(f_{E_g}(t) - f_{sat}(t) \right) f_{soil E \max} [E_0(t) - E_t(t)] & \text{if } f_{sat} < f_{E_g} \\ 0 & \text{if } f_{sat} \geq f_{E_g} \end{cases} \quad (73)$$

where f_{E_g} [-] is the fraction of the landscape (grid cell) that is accessible for transpiration from groundwater, and f_{sat} [-] is the fraction of the landscape (grid cell) that is saturated.

4 Vegetation Phenology

Vegetation stand density (and its effect on leaf area) plays a significant role in the water balance and streamflow generation. Some measure or estimate of vegetation density is therefore crucial for modulating the hydrological processes in AWRA-L. Leaf biomass is dynamically modelled within AWRA-L and is directly related to various vegetation cover metrics including leaf area index LAI and fractional canopy cover f_v .

Leaf biomass M [kg m^{-2}] modulates the following processes in AWRA-L:

- potential evaporation through alteration of albedo (within the energy balance)
- interception through altering the area available for interception and the rate of interception evaporation
- transpiration through altering canopy conductance

The vegetation (or vegetation phenology) model simulates leaf biomass dynamics in response to water availability. This is done under the assumption that the vegetation takes on the maximum density that could be sustained by the available moisture.

The 'equilibrium' leaf mass is estimated by considering the hypothetical leaf mass M_{eq} that corresponds with a situation in which maximum transpiration rate ($E_{t\ max}$ – eq 65) equals maximum root water uptake (U_0 – eq 60). The vegetation moves towards this equilibrium state with a prescribed degree of inertia, representative of alternative phenological strategies.

The seasonal vegetation dynamics model is constrained by the mass balance equation. Mass of vegetation M [kg m^{-2}] is given according:

$$M(t + 1) = M(t) + \Delta t M_n(t) \quad (74)$$

where Δt is the length of the time step [1 day]. M_n is the change in leaf biomass at each time step [$\text{kg m}^{-2} \text{d}^{-1}$] that moves towards the equilibrium leaf mass (M_{eq}) according to:

$$M_n(t) = \begin{cases} \frac{M_{eq}(t) - M(t)}{t_{grow}}, & \text{if } M(t) < M_{eq}(t) \\ \frac{M_{eq}(t) - M(t)}{t_{senc}}, & \text{if } M(t) \geq M_{eq}(t) \end{cases} \quad (75)$$

where t_{grow} [days] is the characteristic time scale for vegetation growth towards equilibrium, t_{senc} [days] is the characteristic time scale for vegetation senescence towards equilibrium. There is little information available in the literature to estimate t_{grow} and t_{senc} . However, they can readily be calibrated to LAI patterns derived from remote sensing. Van Dijk (2010a) notes through visual estimation for around 30 sample locations across Australia, t_{grow} and t_{senc} were both estimated at 50 days for shallow-rooted vegetation, and 90 days for deep-rooted vegetation. However, t_{grow} values of 150 days and 1000 days, and t_{senc} values of 10 days and 60 days have been used for all versions of AWRA-L up until v6 (for shallow and deep rooted vegetation respectively), with the values optimised in v7.

This formulation was developed by Van Dijk (2010c) because literature review did not suggest a suitably simple model that predicts water-related vegetation phenology (see review by Arora (2002)). The formulation is based on the assumption that vegetation is able to adjust its leaf biomass at a rate that is independent of the amount of existing leaf biomass and energy or biomass embodied in other plant organs (a strong simplification of the complex physiological processes).

Fractional canopy cover f_v [-], is related to biomass (M) according to the following dimensional conversion:

$$LAI(t) = M(t) SLA \quad (76)$$

and then:

$$f_v(t) = 1 - \exp\left(-\frac{LAI(t)}{LAI_{ref}}\right) \quad (77)$$

where SLA is the specific leaf area [$m^2 kg^{-1}$] (the ratio of leaf area to dry mass), and LAI_{ref} is the reference leaf area index [-] corresponding to $f_v = 0.632$ (the value of f_v in Eq. (77) when $LAI(t) = LAI_{ref}$).

As Van Dijk (2010a) explains, the conversion from LAI to f_v is described by the exponential light extinction equation (Monsi and Saeki 1953) equivalent to Beer's Law which is most commonly used for this purpose. However, to be consistent with notation elsewhere in the model, the so-called 'light extinction coefficient' (often symbolised by κ) is not used but its inverse value LAI_{ref} is used instead, which represents a reference LAI at which fraction cover is 0.632.

Globally reported values of SLA vary by two orders of magnitude, from 0.7 to 71 [$m^2 kg^{-1}$] (I. J. Wright et al. 2004). Values of 1.5 to 9 $m^2 kg^{-1}$ have been found for Australian Eucalypt species (Schulze et al. 2006) with an average value of approximately 3 $m^2 kg^{-1}$. Fixed values of 10 $m^2 kg^{-1}$ and 3 $m^2 kg^{-1}$ were chosen by Van Dijk (2010a) for shallow and deep-rooted vegetation HRUs respectively.

Maximum achievable canopy cover (f_{vmax}) is given, inverting (62), by:

$$f_{vmax} = 1 - \exp\left(-\frac{\max(LAI_{max}, 0.00278)}{LAI_{ref}}\right) \quad (78)$$

where LAI_{max} is the maximum achievable leaf area index [-]. LAI_{max} is derived from a time series of LAI from the MODIS satellite (Figure 15). At present, the same values of LAI_{max} are used for both HRUs.

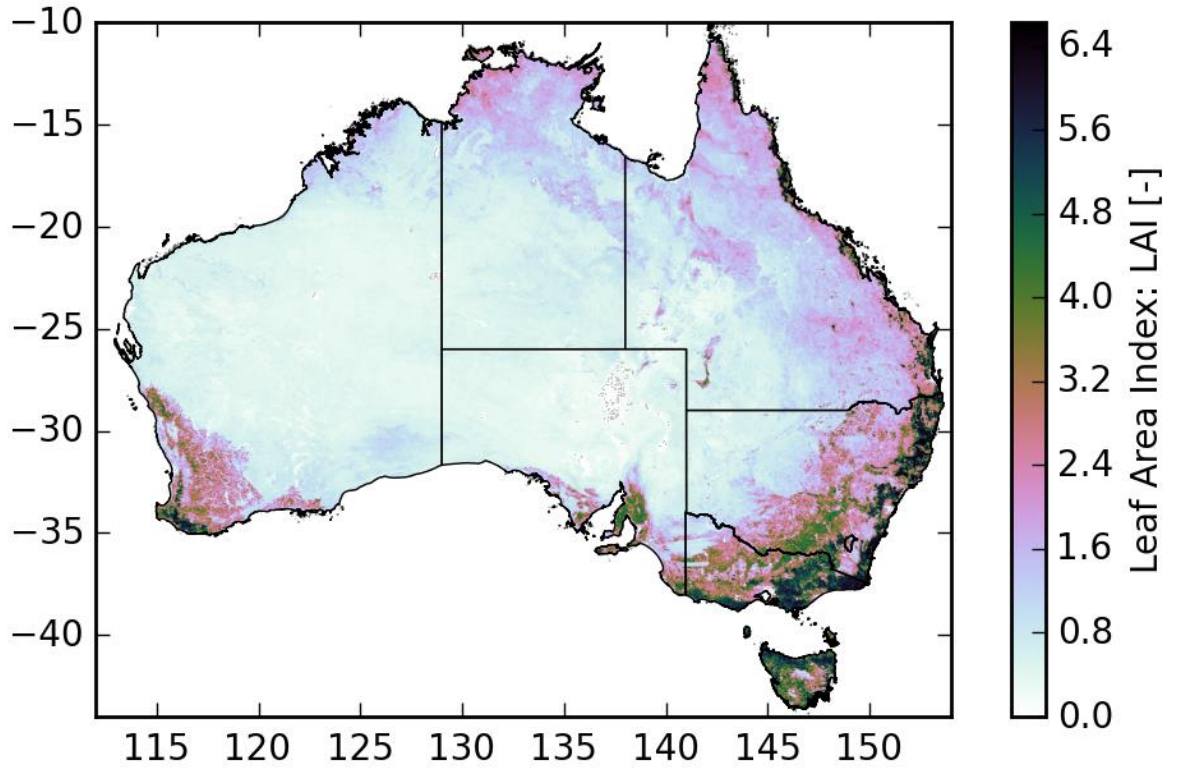


Figure 15. Maximum Leaf Area Index (LAI_{max})

Van Dijk (2010a) derives the equilibrium canopy cover as being given by:

$$f_{veq} = \min \left\{ \left(\frac{U_0(t)}{E_0(t) - U_0(t)} \right) \left(\frac{k_\varepsilon(t)}{1 + k_\varepsilon(t)} \right) \frac{g_a(t)}{c_G V_c}, f_{vmax} \right\} \quad (79a)$$

where the associated equilibrium leaf mass M_{eq} is:

$$M_{eq}(t) = -\frac{LAI_{ref}}{SLA} \ln(1 - f_{veq}(t)) \quad (79b)$$

5 Parameterisation

5.1 Parameterisation of AWRA-L v7

5.1.1 Calibration and evaluation approach

AWRA-L v7 contains 57 notionally optimisable parameters (4 parameters more than v6) – see Table 1. Thirty-six parameters are chosen a priori based through previous experience or according to mapping data – toward reducing the number of parameters to be optimised (and better identifying parameters that the model is sensitive to). The remaining 21 parameters are optimised across the continent to maximise a composite objective function combining the performance according to various water balance datasets. It is noted that only 1 parameter set is used across the whole continent.

Automated calibration is undertaken on the National Computational Infrastructure (NCI; <http://nci.org.au>) supercomputer using distributed simulation of 295 gridded catchments (11320 grid cells), using pre-defined starting states, a full simulation period 01/07/1950 - 30/12/2011, and evaluation period 01/01/1981 - 30/12/2011. The Shuffled Complex Evolution algorithm (Duan, Gupta, and Sorooshian 1993) is used for optimisation with 75,000 function evaluations set as the upper limit. The optimisation was undertaken on NCI High Performance Computers (HPC), with each calibration using 1400 CPUs and 1.13 TB memory for approximately 17 hours (more details about the CPU specifications: <https://nci.org.au/our-systems/hpc-systems>). The calibration was conducted 5 times with different random seed numbers to ensure the optimality of the resulting parameter set, with the final simulation seed chosen according to best objective function value. Input calibration data and defined objective functions were as detailed below.

For evaluation purposes, simulation was from 1950 - 2018, with evaluation for all data sets covering the intersection of the observed data and simulated data. 295 catchments not used in calibration are reserved for catchment based evaluation, and grid based outputs used to compare to point based observations. A range of different statistics are used in calibration and evaluation depending on the data type, with the full extent of the data used for evaluation covering the AWRA-L simulation period. Final model performance compared to previous versions is judged according to summary evaluation statistics, based on data not used in calibration – see Frost et al (2021) for more details.

5.1.2 Calibration and validation data

Streamflow, ET, soil moisture, vegetation fraction, and terrestrial water storage are used in calibration and validation for a set of 295 and 291 unimpaired catchments across Australia (see Figure 16) respectively as follows:

- **Catchment streamflow:** a set of 782 unimpaired catchments with gauged flow records across Australia were collated by Zhang *et al.* (2013) according to the following criteria: (a) catchment area is greater than 50 km², (b) the stream is unregulated (no dams or reservoirs), (c) no major impacts of irrigation and land use, (d) observed record has at least 10 years of data between 1975 and 2011.

The catchments (delineated using the [Bureau's national catchment Geofabric product](#)) were collated towards being used in evaluation. The spatial distribution of catchments reserved for calibration and validation of AWRA-L is shown in Figure 16; with regional divisions showing areas of similar climate. Data from 295 catchments covering the period 1/1/1981-30/12/2011 were used in calibration of AWRA-L while 291 catchments not used in calibration were used for validation (Figure 16). The data set was updated to geofabric version 3 in the AWRA-L v7.

- **Catchment evapotranspiration:** CSIRO MODIS reflectance-based Scaling ET ([CMRSET](#); Guerschman et al., 2009) satellite retrieval based grid estimates of 8-day evapotranspiration covering 2001-2017, where 2001-2011 are used for calibration catchments and 2001-2017 are used for validation catchments.
- **Catchment soil moisture:** ASCAT product (<https://manati.star.nesdis.noaa.gov/datasets/ASCATData.php>) satellite retrieval based grid estimates of soil moisture, covering the period of 2002-2013 have been used where 2002-2011 are used for calibration catchments and 2002-2013 for validation catchments.
- **Terrestrial Water Storage (TWS) anomaly:** represents the water content change within the entire observed soil column at monthly timesteps as observed from GRACE mission satellite covering the period of 2002-2017 where 2002-2011 are used for calibration catchments and 2002-2017 are used for validation catchments.
- **Vegetation fraction (F_{veg}) cover:** provides quantitative information about the vegetation dynamics within a given grid cell. Estimates used here are derived using Moderate-resolution Imaging Spectroradiometer (MODIS) Nadir BRDF-Adjusted Reflectance product (MCD43A4) collection 6 data following Guerschman et al. (2015). The 8-day F_{veg} is used over the periods 2001-2011 for calibration catchments and 2001-2017 for validation catchments.

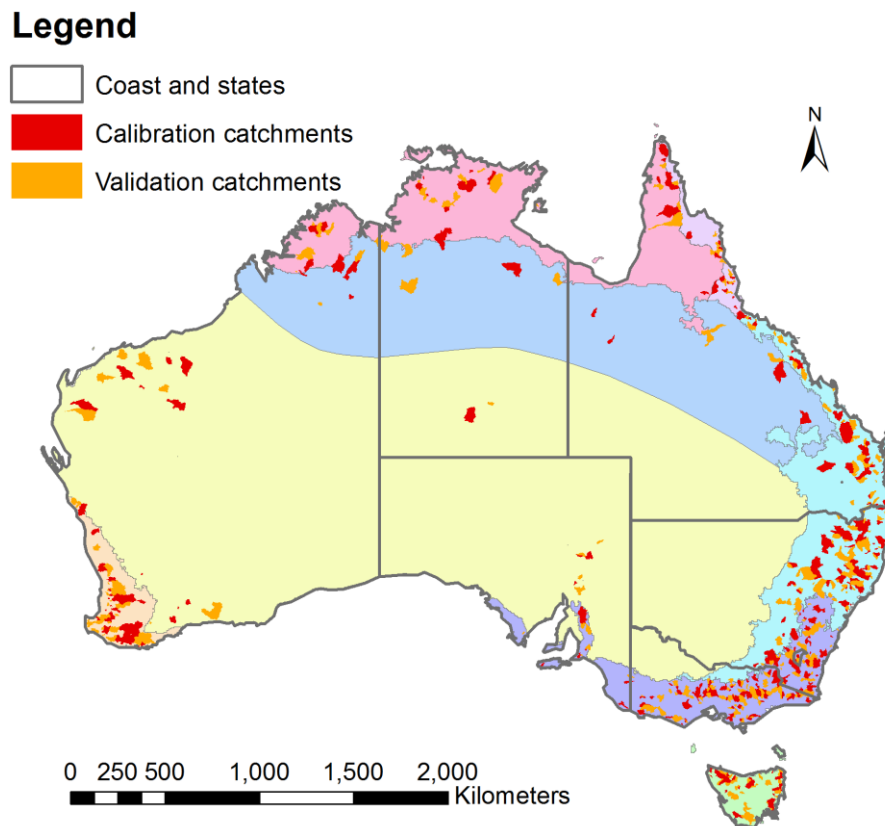


Figure 16. Location of unimpaired catchments used for model evaluation with climate zones overlain.

Lumped versus spatial calibration: A new spatial calibration approach is applied in AWRA-L v7, where model pixel output values are compared against spatially distributed satellite data for soil moisture, ET, F_{veg} and TWS, rather than using lumped catchment average values of evapotranspiration and soil moisture as used in all previous versions of AWRA-L. This change is implemented towards more accurately representing spatial and temporal variability within catchments. The correlation of each pixel of the model is calculated against the observation then the correlations are aggregated across catchments, with the median value weighted according to catchment size.

Statistics used in calibration and evaluation: Various statistics are calculated for each catchment (streamflow), model grid cell (remotely sensed soil moisture, ET, F_{veg} and TWS), or sites for other variables (point based measurements including recharge, soil moisture, and ET) to assess the model's performance depending on the variable type:

Relative bias (B)

$$B_i = \sum_{t=1}^T \frac{Q_{mit} - Q_{oit}}{\bar{Q}_{oi}} \quad (80)$$

Nash-Sutcliffe Efficiency (NSE)

$$NSE_i = 1 - \sum_{t=1}^T \frac{(Q_{mit} - Q_{oit})^2}{(Q_{oit} - \bar{Q}_{oit})^2} \quad (81)$$

Pearson's correlation coefficient (r)

$$r_i = \frac{\sum_{t=1}^T (Q_{oit} - \bar{Q}_{oi})(Q_{mit} - \bar{Q}_{mi})}{\sqrt{\sum_{t=1}^T (Q_{oit} - \bar{Q}_{oi})^2} \sqrt{\sum_{t=1}^T (Q_{mit} - \bar{Q}_{mi})^2}} \quad (82)$$

Where Q_{mit} and Q_{oit} represent the modelled simulations and observations respectively for site/catchment i and timestep t for T available observations. \bar{Q}_{oi} and \bar{Q}_{mi} are the mean of the observations and modelled outputs respectively over all timesteps.

The bias and monthly NSE statistics in particular are seen as good metrics for judging AWRA-L model's performance for simulating streamflow and TWS. Pearson's correlation coefficient is a good indicator for variables where the bias (and absolute value) of the variable is not as important as matching the variability (e.g. soil moisture, actual ET or fraction vegetation).

Calibration objective:

The following streamflow objective function is evaluated for each catchment simulation (as derived by Viney et al., 2009):

$$F_s = NSE_d - 5 | \ln(1 + B) |^{2.5} \quad (83)$$

where NSE_d is the daily Nash-Sutcliffe Efficiency (eq. 81) and B is relative bias. Since the calibration and validation catchments are small enough, and there is no routing process in AWRA-L currently, the runoff aggregated to catchment boundaries is compared to streamflow.

In addition to F_s for streamflow in calibration daily soil moisture correlation (r_{sm}), 8-day evapotranspiration correlation (r_{et}), 8-day fraction vegetation correlation (r_{fveg}) and monthly NSE of de-seasonalised TWS (NSE_{dsTWS}) are calculated (by subtracting monthly means from TWS timeseries) for each catchment for each catchment as different components of the objective function. For TWS, the influence of leakage and highly uncertain data on coastal areas is dealt with using reduced weighting when a GRACE pixel has area covered by the Ocean. The weight of a pixel is reduced proportionally with reduction of the GRACE pixel land coverage (see Fig 6 in Frost et al., 2021).

In the case of the spatially varying data within a catchment, the median value of the statistic is calculated across all cells within each catchment and then the median value

is weighted according to the number of cells in each catchment (a proxy for catchment area).

Performance across the calibration catchments is then averaged for each variable type by using the following average:

$$OF_{cm} = \text{mean} (OF_{cm25\%}, OF_{cm50\%}, OF_{cm75\%}, OF_{cm100\%}) \quad (84)$$

where $OF_{cmX\%}$ is the X_{th} ranked average percentile OF_{cm} value for each catchment objective where $cm \in c = F_s, r_{sm}, r_{et}, r_{fveg}, NSE_{dsTWS}$.

This objective function aims to get an adequate fit over a wide range of sites, but also to exclude very poor fitting areas (i.e. those below the 25%), possibly influenced by poor data. Finally, the calibration of AWRA-L maximises the grand objective function across all variables as:

$$\text{grandOF} = 50\% NSE_{dsTWS} + 35\% F_s + 7.5\% r_{sm} + 2.5\% r_{et} + 5\% r_{fveg} \quad (85)$$

Weighting for streamflow has been reduced to 35%, satellite-derived soil moisture to 7.5%, evapotranspiration to 2.5% and vegetation fraction to 5%. This modified grand objective function in v7 provides better constraints for the overall model calibration of all water balance components and vegetation. This weighting is a marked change from AWRA-L v6 with large weighting now applied on TWS (weighted 50%) along with the addition of vegetation fraction, where previously the focus was on streamflow (weighted 70%) with lower weights applied to satellite derived soil moisture and evapotranspiration (15% each). The weights were obtained as a result trial and error tests, starting from the previous model weighting scheme.

In addition to the optimised parameters, some parameters were manually tuned/specified during experimentation and differ from previous versions. The following parameters were manually tuned/specified during experimentation and differ from previous versions (Table 1): Dry and Wet soil albedo (α_d, α_w), Reference leaf area index (LAI_{ref}), Specific leaf area (SLA), Characteristic time scale for vegetation growth and senescence towards equilibrium (t_{grow}, t_{senc}), Vegetation photosynthetic capacity index per unit canopy cover (V_c), Scale for the fraction of impervious area (f_{imp_scale}). It is noted that some optimised vegetation parameters in version 7 are currently outside of physically realistic bounds (eg. t_{grow}, t_{senc} , SLA). For further details of calibration, evaluation of model performance and a-priori specification of model parameters see Viney *et al.* (2015), Frost and Wright (2018b, 2018a), Frost *et al.* (2021) and Van Dijk (2010c).

Table 1. AWRA-L v5, v6 and v7 parameter values. Values that are optimised are shown in bold. Values manually-tuned/specified are presented with an underline

Symbol		AWRA Lv5		AWRA-L v6		AWRA-L v7			Unit
		Deep	Shallow	Deep	Shallow	Deep	Shallow	Imp	
α_d	Dry soil albedo	0.26	0.26	0.26	0.26	0.18	0.18	-	-
α_w	Wet soil albedo	0.16	0.16	0.16	0.16	0.08	0.08	-	-
c_G	Photosynthetic capacity conversion coeff.	0.032	0.024	0.021	0.032	0.043	0.028	0	m/s
f_{ER}	Average evaporation rate over average rainfall intensity during storms per unit canopy	0.074	0.5	0.074	0.5	0.130	0.5	0	-
F_{smax}	Soil evaporation scaling factor when soil water supply is not limiting evaporation	0.227	0.929	0.585	0.999	0.998	0.816	0	-
h_{avg}	Height of vegetation canopy	Grid	0.5	Grid	0.5	Grid	0.5	0	m
LAI_{ref}	Reference leaf area index (at which $f_v = 0.63$)	2.5	1.4	2.5	1.4	6.537	4.562	0	-
SLA	Specific leaf area	3	10	3.0	10	297.3	378.3	0	m ² /kg
s_l	Specific canopy storage capacity per leaf area	0.094	0.042	0.067	0.292	0.048	0.273	0	mm
t_{grow}	Characteristic time scale for vegetation growth	1000	150	1000	150	325.33	16.84	0	days
t_{senc}	Characteristic time scale for veg. senescence	60	10	60	10	1.65	50.38	0	days
U_{s0}	Shallow soil Max. root water uptake rates	0	6	0	6	6	6	0	mm/d
U_{d0}	Deep soil Max. root water uptake rates	7.13	0	11.569	0	grid	0	0	mm/d
V_c	Photosynthetic capacity per unit canopy cover	0.35	0.65	0.35	0.65	0.177	0.265	0	-
w_{ref}	Topsoil water content that evaporation is reduced	0.85	0.85	0.85	0.85	0.85	0.85	0	-
w_{slim}	Water-limiting water content in shallow store	0.3	0.3	0.3	0.3	0.3	0.3	0	-
w_{dlim}	Water-limiting water content deep store	0.3	0.3	0.3	0.3	0.3	0.3	0	-
D_R	Rooting depth	6	1	6	1	6	1	0	m
ξ_0	Baseflow threshold factor	-	-	-	-	-	6.487	-	mm
μ_0	Baseflow shape factor	-	-	-	-	-	16.018	-	-
$K_{gw\ scale}$	Multiplier on the raster input of K_{gw}	0.502	-	0.939	-	-	9.010	-	-
$K_{gw\ power}$	Power factor on the raster input of K_{gw}	-	-	-	-	-	2.557	-	-
K_{rint}	Intercept for routing coefficient K_r	0.157	-	0.165	-	-	0.081	-	-
$K_{r\ scale}$	Scale for routing coefficient K_r	0.05	-	0.048	-	-	0.081	-	-
k_β	Coefficient on the mapped slope for interflow	0.951	-	0.438	-	-	0.149	-	-
k_ζ	K_{sat} ratio coefficient for interflow	0.074	-	0.661	-	-	0.493	-	-
$K_{0\ sats\ scale}$	Saturated hydraulic cond. scale top layer	2.872	-	3.892	-	-	8.307	-	-
$K_{s\ sats\ scale}$	Saturated hydraulic cond. scale shallow layer	0.02	-	0.052	-	-	0.016	-	-
$K_{d\ sats\ scale}$	Saturated hydraulic cond. scale in deep layer	0.01	-	0.012	-	-	0.043	-	-
m	Weight for averaging the k_{sat} of the first layer	0.5	-	1	-	-	0.666	-	-
$MTTPT$	Maximum Tree Transpiration per basal area	-	-	-	-	-	0.084	-	-
n_{scale}	Scale for effective porosity	0.055	-	0.042	-	-	0.029	-	-
$P_{ref\ scale}$	Multiplier on the raster input of P_{ref}	1.815	-	2.564	-	-	2.637	-	-
$S_{0\ max\ scale}$	Maximum water storage scale surface layer	2.995	-	2.804	-	-	2.465	-	-
$S_{s\ max\ scale}$	Maximum water storage scale shallow layer	2.433	-	1.993	-	-	1.638	-	-
$S_{d\ max\ scale}$	Maximum water storage scale deep layer	0.795	-	0.884	-	-	0.904	-	-
$f_{imp\ scale}$	Scale for the fraction of impervious area	-	-	-	-	-	0.5	-	-

6 Conclusion

This report details the Australian Water Resource Assessment Model version 7. This model builds on previous development of AWRA by CSIRO, the Bureau of Meteorology and various research partners over the last decade towards better monitoring and water resource modelling.

Various changes were implemented in version 7 compared to previous versions of AWRA-L including altering the inputs, altering the model conceptual structure, and altering the calibration approach.

The changes in static and dynamic inputs improves the performance of AWRA-L, particularly for ET fluxes, as described in a companion evaluation report (Frost et al. 2021).

Key changes from a conceptual perspective include (a) incorporation of impervious hydrological response unit providing better performance for urban catchments (b) addition of a baseflow cutoff process for better representation of ephemerality of streamflow, and (c) an alteration of the top layer soil drainage parameterisation to better represent daily variability. These changes result in better streamflow performance nationally and for urban catchments, along with better performance for top layer soil moisture (see Frost et al. 2021).

The new spatial calibration procedure employed, using terrestrial water storage (from GRACE) and fraction of vegetation (from MODIS) in addition to streamflow, ET and soil moisture, allows better constraining of the model according to the whole water balance. This approach, coupled with the conceptual changes implemented, allows better performance of AWRA-L for streamflow than was previously possible (even though it is weighted lower in the overall calibration objective - 35% compared to 70% previously), while vegetation, total water storage and other evaluation metrics also improve (see Frost et al. 2021).

As a result of these changes and the improved performance described in a companion evaluation report (Frost et al. 2021), AWRA v7 is recommended for operational use by the Bureau of Meteorology for water resource monitoring, forecasting and assessment purposes over AWRA-L v6.

References

- Allen, Richard G., L.S. Pereira, D. Raes, and M. Smith. 1998. 'Crop Evapotranspiration: Guidelines for Computing Crop Requirements'. *Irrigation and Drainage Paper No. 56*, FAO (56): 300.
- Armston, John David et al. 2009. 'Prediction and Validation of Foliage Projective Cover from Landsat-5 TM and Landsat-7 ETM+ Imagery'. *Journal of Applied Remote Sensing* 3(1): 1–28. <https://doi.org/10.1117/1.3216031>.
- Arora, Vivek. 2002. 'Modeling Vegetation as a Dynamic Component in Soil-Vegetation-Atmosphere Transfer Schemes and Hydrological Models'. *Reviews of Geophysics* 40(2): 1–26.
- Brunt, D. 1932. 'Notes on Radiation in the Atmosphere. I'. *Quarterly Journal of the Royal Meteorological Society* 58(247): 389–420.
- Brutsaert, Wilfried. 1975. 'On a Derivable Formula for Long-Wave Radiation from Clear Skies'. *Water Resources Research* 11(5): 742–44.
- Dane, J H, and W Puckett. 1994. 'Field Soil Hydraulic Properties Based on Physical and Mineralogical Information'. In *International Workshop on Indirect Methods for Estimating the Hydraulic Properties of Unsaturated Soils*, ed. MTh van Genuchten et al. Riverside, CA: University of California, 389–403.
- Van Dijk, A. I J M, and L. A. Bruijnzeel. 2001. 'Modelling Rainfall Interception by Vegetation of Variable Density Using an Adapted Analytical Model. Part 1. Model Description'. *Journal of Hydrology* 247(3–4): 230–38.
- Van Dijk, Albert I J M. 2010a. 'Climate and Terrain Factors Explaining Streamflow Response and Recession in Australian Catchments'. *Hydrology and Earth System Sciences* 14(1): 159–69. <http://www.hydrol-earth-syst-sci.net/14/159/2010/> (November 18, 2016).
- . 2010b. 'Selection of an Appropriately Simple Storm Runoff Model'. *Hydrology and Earth System Sciences* 14(3): 447–58. <http://www.hydrol-earth-syst-sci.net/14/447/2010/hess-14-447-2010.pdf> (November 18, 2016).
- . 2010c. *The Australian Water Resources Assessment System. Technical Report 3. Landscape Model (Version 0.5) Technical Description*. CSIRO: Water for a Healthy Country National Research Flagship.
- Dong, A, S R Grattan, J J Carroll, and C R K Prashar. 1992. 'Estimation of Daytime Net Radiation Over Well Watered Grass'. *Journal of Irrigation and Drainage Engineering* 118(3): 466–79.
- Donohue, Randall J, Tim R McVicar, and Michael L Roderick. 2009. *Generating Australian Potential Evaporation Data Suitable for Assessing the Dynamics in Evaporative Demand within a Changing Climate*. CSIRO: Water for a Healthy Country National Research Flagship.

- Donohue, Randall J, Michael L Roderick, and Tim R McVicar. 2008. 'Deriving Consistent Long-Term Vegetation Information from AVHRR Reflectance Data Using a Cover-Triangle-Based Framework'. *Remote Sensing of Environment* 112(6): 2938–49. <http://www.sciencedirect.com/science/article/pii/S0034425708000618>.
- Duan, Q Y, V K Gupta, and S Sorooshian. 1993. 'Shuffled Complex Evolution Approach for Effective and Efficient Global Minimization'. *Journal of Optimization Theory and Applications* 76(3): 501–21. <http://dx.doi.org/10.1007/BF00939380>.
- Duffie, John A, and William A Beckman. 2013. *Solar Engineering of Thermal Processes Solar Engineering*. 4th ed. Hoboken, New Jersey: Wiley.
- Elmahdi, Amgad; et al. 2015. 'Australian Water Resources Assessment Modelling System (AWRAMS)-Informing Water Resources Assessment and National Water Accounting'. *36th Hydrology and Water Resources Symposium: The art and science of water. Barton, ACT: Engineers Australia*: 979–86.
- Fröhlich, C., and R.W. Brusa. 1981. 'Solar Radiation and Its Variation in Time'. *Solar Physics* 74: 209–15.
- Frost, A.J. et al. 2021. *Evaluation of the Australian Landscape Water Balance Model: AWRA-L V7*.
- Frost, A.J., and D.P. Wright. 2018a. *Evaluation of the Australian Landscape Water Balance Model (AWRA-L v6): Comparison of AWRA-L v6 against Observed Hydrological Data and Peer Models*.
- . 2018b. 'The Australian Water Resource Assessment Landscape Model – AWRA-L: Improved Performance and Regional Calibration'. In *Proceedings from HWRS2018: Hydrology and Water Resources Symposium, Melbourne*.
- Gallant, John C, and Trevor I Dowling. 2003. 'A Multiresolution Index of Valley Bottom Flatness for Mapping Depositional Areas'. *Water Resources Research* 39(12). <https://doi.org/10.1029/2002WR001426>.
- Gash, J. H. C. 1979. 'An Analytical Model of Rainfall Interception by Forests'. *Quarterly Journal of the Royal Meteorological Society* 105(443): 43–55.
- Gash, J H C, C R Lloyd, and G Lachaudb. 1995. 'Estimating Sparse Forest Rainfall Interception with an Analytical Model'. *Journal of Hydrology* 170(95): 79–86.
- Gill, Tony et al. 2017. 'A Method for Mapping Australian Woody Vegetation Cover by Linking Continental-Scale Field Data and Long-Term Landsat Time Seriesfile'. *International Journal of Remote Sensing* 38(3): 679–705. <https://doi.org/10.1080/01431161.2016.1266112>.
- Grant, I. et al. 2008. 'Meteorological and Remotely Sensed Datasets for Hydrological Modelling: A Contribution to the Australian Water Availability Project'. In *Proceedings of the Catchment-Scale Hydrological Modelling & Data Assimilation (CAHMDA-3) International Workshop on Hydrological Prediction: Modelling, Observation and Data Assimilation*,

January 9 2008–January 11 2008,.

- Guerschman, Juan P et al. 2015. 'Assessing the Effects of Site Heterogeneity and Soil Properties When Unmixing Photosynthetic Vegetation, Non-Photosynthetic Vegetation and Bare Soil Fractions from Landsat and MODIS Data'. *Remote Sensing of Environment* 161: 12–26. <https://www.sciencedirect.com/science/article/pii/S0034425715000395>.
- Hafeez, Mohsin et al. 2015. 'The Bureau's Operational AWRA Modelling System in the Context of Australian Landscape and Hydrological Model Products'. *36th Hydrology and Water Resources Symposium* (December).
- Iqbal, Muhammad. 1983. *An Introduction to Solar Radiation*.
- Jensen, M E, J L Wright, and B J Pratt. 1971. 'Estimating Soil Moisture Depletion from Climate, Crop and Soil Data'. *Transaction of the ASAE* 14(5): 954–59.
- Jones, D A, William Wang, and Robert Fawcett. 2009. 'High-Quality Spatial Climate Data-Sets for Australia'. *Australian Meteorological and Oceanographic Journal* 58: 233–48.
- Liu, Benjamin Y.H., and Richard C. Jordan. 1960. 'The Interrelationship and Characteristic Distribution of Direct, Diffuse and Total Solar Radiation'. *Solar Energy* 4(3): 1–19.
- McVicar, T R et al. 2008. 'Wind Speed Climatology and Trends for Australia, 1975-2006: Capturing the Stilling Phenomenon and Comparison with near-Surface Reanalysis Output'. *Geophysical Research Letters* 35(L20403).
- Minasny, Budiman, and Alex. B McBratney. 2000. 'Evaluation and Development of Hydraulic Conductivity Pedotransfer Functions for Australian Soil'. *Soil Research* 38(4): 905–26. <https://doi.org/10.1071/SR99110>.
- Minasny, Budiman, Alex B McBratney, and Keith L Bristow. 1999. 'Comparison of Different Approaches to the Development of Pedotransfer Functions for Water-Retention Curves'. *Geoderma* 93(3): 225–53. <http://www.sciencedirect.com/science/article/pii/S0016706199000610>.
- Monsi, Masami, and Toshiro Saeki. 1953. 'Über Den Lichtfaktor in Den Pflanzengesellschaften Und Seine Bedeutung Für Die Stoffproduktion'. *Japanese Journal of Botany* 14: 22–52.
- Owens, J. et al. 2019. 'Improving Evapotranspiration Estimation in Pasture and Native Vegetation Models Using Flux Tower Data, Remote Sensing and Global Optimisation'. In *23rd International Congress on Modelling and Simulation - Supporting Evidence-Based Decision Making: The Role of Modelling and Simulation, MODSIM 2019*, , 414–20.
- Peeters, L J M, R S Crosbie, R C Doble, and A I J M Van Dijk. 2013. 'Conceptual Evaluation of Continental Land-Surface Model Behaviour'. *Environmental Modelling & Software* 43(0): 49–59. <http://www.sciencedirect.com/science/article/pii/S1364815213000200>.
- Penman, H.L. 1948. 'Natural Evaporation from Open Water, Bare Soil and Grass'. *The Royal Society* 193(1032): 120–45.
- Raupach, M R et al. 2008. *Australian Water Availability Project (AWAP) - CSIRO Marine and*

Atmospheric Research Component: Final Report for Phase 3. Caberra, Australia: CSIRO Marine and Atmospheric Research.

- Roderick, Michael L. 1999. 'Estimating the Diffuse Component from Daily and Monthly Measurements of Global Radiation'. *Agricultural and Forest Meteorology* 95(3): 169–85.
- Schulze, Ernst Detlef, Neil C. Turner, Dean Nicolle, and Jens Schumacher. 2006. 'Species Differences in Carbon Isotope Ratios, Specific Leaf Area and Nitrogen Concentrations in Leaves of Eucalyptus Growing in a Common Garden Compared with along an Aridity Gradient'. *Physiologia Plantarum* 127(3): 434–44.
- Shuttleworth, W.J. 1992. 'Chapter 4. Evaporation'. In *'Handbook of Hydrology'*, ed. D.R. Maidment. , 4.1-4.53.
- Simard, Marc, Naiara Pinto, Joshua B Fisher, and Alessandro Baccini. 2011. 'Mapping Forest Canopy Height Globally with Spaceborne Lidar'. *Journal of Geophysical Research: Biogeosciences* 116(G4): G04021. <http://dx.doi.org/10.1029/2011JG001708>.
- Spencer, J. W. 1971. 'Fourier Series Representation of the Position of the Sun'. *Search* 2(5): 172.
- Thom, A.S. 1975. '3. Momentum, Mass and Heat Exchange of Plant Communities'. In *Vegetation and the Atmosphere: Principles*, , 57.
- Vaze, J. et al. 2018. *AWRA-L Input Spatial Layers at 1 Km and 5 Km Resolutions for the Australian Continent - Source Data and Comparison between 1 Km and 5 Km Resolutions*.
- Vaze, J et al. 2013. 'The Australian Water Resource Assessment System (AWRA)'. In *Proceedings of the 20th International Congress on Modelling and Simulation*, Adelaide, Australia.
- Viney, N et al. 2015. *AWRA-L v5.0: Technical Description of Model Algorithms and Inputs*. CSIRO, Australia.
- Viney, Neil R et al. 2014. 'The AWRA Modelling System'. *Hydrology and Water Resources Symposium 2014*: 1018–25. <http://search.informit.com.au/documentSummary;dn=388600432195626;res=IELENG>.
- Wright, I J et al. 2004. 'The Worldwide Leaf Economics Spectrum'. *Nature* 428: 821–27.
- Wright, J L, and M E Jensen. 1972. 'Peak Water Requirements of Crops in Southern Idaho'. *Journal of the Irrigation and Drainage Division* 98(IR2): 193–201.
- Wright, James L. 1982. 'New Evapotranspiration Crop Coefficients'. *Journal of the Irrigation and Drainage Division* 108(1): 57–74.
- Zhang, Y Q et al. 2013. *Collation of Streamflow and Catchment Attribute Dataset for 780 Unregulated Australian Catchments*. CSIRO: Water for a Healthy Country National Research Flagship.

Appendices

Appendix A: Table of model variables

Appendix B: Downward longwave radiation derivation

Appendix A: Table of model variables

Table 2. List of variable names used in this document and the corresponding variables used in the model code. Units are those given in this document.

Document	Model code	Description
A_0	A	Availability factor for releasing groundwater baseflow (dimensionless)
α	alb	Surface albedo (dimensionless)
α_{dry}	alb_dry	Dry soil albedo (dimensionless)
α_s	alb_soil	Albedo of soil surface (dimensionless)
α_v	alb_veg	Albedo of vegetated surfaces (dimensionless)
α_{wet}	alb_wet	Wet soil albedo (dimensionless)
β	slope	Slope of the land surface (percent)
γ	gamma	Psychrometric constant (Pa K ⁻¹)
Δ	delta	Slope of the saturation vapour pressure curve (Pa K ⁻¹)
δ	DELTA	Solar declination (radians)
λ	lambda	Latent heat of vaporisation (MJ kg ⁻¹)
λ_d	Dd	Surface water drainage density (m ⁻¹)
ρ_0	Rh_0s	Partitioning factor for vertical and lateral drainage from the surface soil layer (dimensionless)
ρ_s	Rh_sd	Partitioning factor for vertical and lateral drainage from the shallow soil layer (dimensionless)
σ	StefBolz	Stefan-Boltzmann constant (MJ m ⁻² d ⁻¹ K ⁻⁴)
ϕ	latitude	Latitude (radians), and is negative in the southern hemisphere
ω	PI	Sunset hour angle (radians)
$c_{g_s,max}$	cGsmax	Coefficient relating vegetation photosynthetic capacity to maximum stomatal conductance (m s ⁻¹)
D_0	D0	Vertical drainage from the bottom of the surface soil layer (mm)
D_d	Dd	Vertical drainage from the bottom of the deep soil layer (mm)
D_R	RD	Rooting depth (m)
D_s	Ds	Vertical drainage from the bottom of the shallow soil layer (mm)
DOY	DayOfYear	Day of the year (d)
d_0	—	Depth of the top soil layer (mm)
d_d	—	Depth of the deep soil layer (mm)
d_s	—	Depth of the shallow soil layer (mm)
d_u	—	Depth of the unconfined aquifer (m)
E_0	E0	Potential evaporation (mm d ⁻¹)
\bar{E}^*	meanpet	Long term mean daily potential evaporation (mm d ⁻¹)
E_s	Es	Evaporation flux from the surface soil store (mm d ⁻¹)
E_g	Eg	Evaporation flux from the groundwater store (mm d ⁻¹)
E_i	Ei	Evaporation flux from canopy interception (mm d ⁻¹)
E_t	Et	Actual total transpiration flux (mm d ⁻¹)
$E_{t,max}$	Etmax	Potential transpiration rate (mm d ⁻¹)
E_{tot}	Etot	Total evapotranspiration (mm d ⁻¹)
ξ_0	baseflow_thr	Baseflow threshold factor (dimensionless)
F_{ERO}	ER_frac_ref	Specific ratio of the mean evaporation rate and the mean rainfall intensity during storms
$f_{soil E}$	fsoile	Relative soil evaporation
$f_{soil E max}$	fsoilemax	Soil evaporation scaling factor corresponding to unlimited soil water supply (dimensionless)
f_{ig}	fEgt	Fraction of the grid cell that is accessible for transpiration from groundwater (dimensionless)
f_{er}	fer	ratio of average evaporation rate to average rainfall intensity (during storms)
f_{sat}	fsat	Fraction of the grid cell that is saturated at the surface (dimensionless)
f_{tree}	f_tree	Fraction of tree cover within each grid cell (dimensionless)
f_r	fveg	Fractional canopy cover (dimensionless)
f_{veg}	fveq	Equilibrium canopy cover (dimensionless)

<i>fPAR</i>	—	Photosynthetically-active radiation (dimensionless)
<i>FPC</i>	FPC	Foliage projected cover (dimensionless)
<i>g_a</i>	ga	Aerodynamic conductance (m s ⁻¹)
<i>g_s</i>	gs	Canopy conductance (m s ⁻¹)
<i>H_b</i>	—	Drainage base – the lowest topographic point within the grid cell (m)
<i>h</i>	—	Elevation of a point on the hypsometric curve (m)
<i>h_u</i>	—	Elevation change along the flow path (m)
<i>h_{veg}</i>	hveg	Vegetation height (m)
<i>I</i>	I	Infiltration (mm)
<i>K_{0sat}</i>	K0sat	Saturated hydraulic conductivity of surface soil layer (mm d ⁻¹)
<i>K_{0satscale}</i>	K0sat_scale	Scaling factor for hydraulic conductivity of surface soil layer(dimensionless)
<i>K_{0satPEDO}</i>	K0sat_grid	Saturated hydraulic conductivity of surface soil layer from pedtransfer(mm d ⁻¹)
<i>K_d</i>	Rgeff	Daily downwelling shortwave (solar) radiation (MJ m ⁻² d ⁻¹)
<i>K_{d0}</i>	RadClearSky	Expected downwelling shortwave radiation on a cloudless day (MJ m ⁻² d ⁻¹)
<i>K_{dsat}</i>	Kdsat	Saturated hydraulic conductivity of deep soil layer (mm d ⁻¹)
<i>K_{dsatPEDO}</i>	Kdsat_grid	Saturated hydraulic conductivity of deep soil layer from pedotransfer (mmd ⁻¹)
<i>K_{dsatscale}</i>	Kdsat_scale	Scaling factor for hydraulic conductivity of deep soil layer (dimensionless)
<i>K_{gmap}</i>	K_gw_grid	Groundwater drainage coefficient obtained from continental mapping (d ⁻¹)
<i>K_{gscale}</i>	K_gw_scale	Scaling factor for groundwater drainage coefficient (dimensionless)
<i>K_g</i>	K_gw	Groundwater drainage coefficient (d ⁻¹)
<i>K_{gpower}</i>	K_gw_power	Power factor for groundwater drainage coefficient (dimensionless)
<i>K_r</i>	K_rout	Rate coefficient controlling discharge to stream (dimensionless)
<i>K_{rint}</i>	Krout_int	Intercept coefficient for calculating <i>K_r</i> (dimensionless)
<i>K_{rscale}</i>	K_rout_scale	Scale coefficient for calculating <i>K_r</i> (d mm ⁻¹)
<i>K_{ssat}</i>	Kssat	Saturated hydraulic conductivity of shallow soil layer (mm d ⁻¹)
<i>K_{ssatPEDO}</i>	Kssat_grid	Saturated hydraulic conductivity of shallow soil layer from pedotransfer (mm d ⁻¹)
<i>K_{ssatscale}</i>	Kssat_scale	Scaling factor for hydraulic conductivity of shallow soil layer (dimensionless)
<i>K_u</i>	—	Daily upwelling shortwave radiation (MJ m ⁻² d ⁻¹)
<i>k_β</i>	slope_coeff	Scaling factor for slope (dimensionless)
<i>k_u</i>	—	Hydraulic conductivity of the unconfined aquifer (m d ⁻¹)
<i>k_ζ</i>	Kr_coeff	Scaling factor for ratio of saturated hydraulic conductivity (dimensionless)
<i>LAI</i>	LAI	Leaf area index (LAI) (dimensionless)
<i>LAI_{max}</i>	LAI _{max}	Maximum achievable LAI value (dimensionless)
<i>LAI_{ref}</i>	LAI _{ref}	Reference LAI value corresponding to <i>f_v</i> = 0.63 (dimensionless)
<i>L_d</i>	RLin	Daily downwelling longwave radiation (MJ m ⁻² d ⁻¹)
<i>L_u</i>	RLout	Daily upwelling longwave radiation (MJ m ⁻² d ⁻¹)
<i>m</i>	k0sat_weight	Weight for averaging the <i>k_{sat}</i> of the first layer (dimensionless)
<i>M</i>	Mleaf	Leaf biomass (kg m ⁻²)
<i>M_{eq}</i>	—	Equilibrium leaf biomass (kg m ⁻²)
<i>M_n</i>	Mleafnet	Change in leaf biomass at each time step (kg m ⁻² d ⁻¹)
<i>MTTPT</i>	mttpt	Maximum Tree Transpiration Per Tree basal area (mm/m ² /ha)
<i>μ₀</i>	baseflow_shape	Baseflow shape factor (dimensionless)
<i>n</i>	ne	Effective porosity (dimensionless)
<i>n_{map}</i>	—	Effective porosity obtained from continental mapping (dimensionless)
<i>n_{scale}</i>	ne_scale	Scaling factor for effective porosity (dimensionless)
<i>P_{wet}</i>	Pwet	Reference threshold precipitation amount (mm)
<i>P_g</i>	Pg	Gross precipitation (mm)

P_n	Pn	Net precipitation – precipitation minus interception (mm)
P_{ref}	PrefR	Reference value for precipitation (mm)
P_{refmap}	—	Mapped reference value for precipitation (mm) prior to scaling
$P_{refscale}$	Pref_gridscale	Scaling factor for reference precipitation (dimensionless)
p_e	pe	Actual vapour pressure (Pa)
p_{es}	pes	Saturation vapour pressure (Pa)
Q_g	Qg	Groundwater discharge to the surface water (mm)
Q_h	Rhof	Infiltration-excess runoff component (mm)
Q_{IF}	QIF	Interflow (mm)
Q_{I0}	IF0	Interflow draining laterally from the surface soil layer (mm)
Q_{Is}	IFs	Interflow draining laterally from the shallow soil layer (mm)
Q_R	QR	Surface runoff (mm)
Q_s	Rsof	Saturation-excess runoff component (mm)
Q_t	Qtot	Total discharge to stream (mm)
R_n	Rneff	Daily net radiation ($\text{MJ m}^{-2} \text{d}^{-1}$)
SLA	SLA	Specific leaf area ($\text{m}^2 \text{kg}^{-1}$)
S_0	S0	Water storage in the surface soil layer (mm)
S_{0AWC}	S0fracAWC_grid	Available water holding capacity in the surface soil (dimensionless)
S_{0max}	S0max	Maximum storage of the surface soil layer (mm)
$S_{0maxscale}$	S0max_scale	Scaling parameter for maximum storage of the surface soil layer(dimensionless)
S_d	Sd	Water content of the deep soil store (mm)
S_{dmax}	Sdmax	Maximum storage of the deep soil layer (mm)
$S_{dmaxscale}$	Sdmax_scale	Scaling parameter for maximum storage of the deep soil layer(dimensionless)
S_g	Sg	Groundwater storage in the unconfined aquifer (mm)
S_r	Sr	Volume of water in the surface water store (mm)
S_s	Ss	Water content of the shallow soil store (mm)
S_{sAWC}	SfracAWC_grid	Available water holding capacity in the shallow soil (dimensionless)
S_{smax}	Ssmax	Maximum storage of the shallow soil layer (mm)
$S_{smaxscale}$	Ssmax_scale	Scaling parameter for maximum storage of the shallow soil layer (dimensionless)
S_{leaf}	S_sls	Specific canopy rainfall storage per unit leaf area (mm)
S_{veg}	sveg	Canopy rainfall storage capacity (mm)
T	-	Surface temperature (K)
T_a	Ta	Daily mean temperature ($^{\circ}\text{C}$)
T_{max}	Tmax	Maximum air temperature ($^{\circ}\text{C}$)
TBA	TBA	Tree basal area (m^2/ha)
T_{min}	Tmin	Minimum air temperature ($^{\circ}\text{C}$)
t	—	Time step (d)
τ_{max}	—	Weight for averaging T_{min} and T_{max} (dimensionless)
Δt	—	Length of the time step (d)
t_{grow}	Tgrow	Characteristic time scale for vegetation growth towards equilibrium (d)
t_{senc}	Tsenc	Characteristic time scale for vegetation senescence towards equilibrium(d)
U_0	U0	Maximum root water uptake (mm d^{-1})
U_d	Ud	Root water uptake (transpiration) from the deep soil store (mm d^{-1})
U_{dmax}	Udmax	Maximum root water uptake from the deep soil store at prevailing moisture content (mm d^{-1})
U_s	Us	Root water uptake (transpiration) from the shallow soil store (mm d^{-1})
U_{smax}	Usmax	Maximum root water uptake from the shallow soil store at prevailing moisture content (mm d^{-1})
u_2	u2	Wind speed at a height of 2 m (m s^{-1})
V_c	Vc	Vegetation photosynthetic capacity per unit canopy cover

w_0	w0	Relative soil moisture content of the top soil layer (dimensionless)
w_{0limE}	w0limE	Limiting the value of w_0 at which evaporation is reduced (dimensionless)
w_{0ref}	w0ref_alb	Reference value of w_0 that determines the rate of albedo decrease with wetness (dimensionless)
w_d	wd	Relative water content of the deep soil store (dimensionless)
w_{dlim}	wdlimU	Water-limiting relative water content of the deep soil store(dimensionless)
w_s	ws	Relative water content of the shallow soil store(dimensionless)
w_{slim}	wslimU	Water-limiting relative water content of the shallow soil store(dimensionless)
Y	Y	Root water uptake (transpiration) from the groundwater store (mm d ⁻¹)

Appendix B: Downward longwave radiation derivation

The downward longwave radiation L_d [W/m²] is derived from the net incoming longwave radiation $R_{ln\ in}$ [W/m²] and the upward longwave radiation L_u [W/m²] as (Shuttleworth 1992)

$$R_{ln\ in}(t) = L_d(t) - L_u(t) \quad (B1)$$

with net outgoing longwave radiation $R_{ln\ out}$ [W/m²], a negative flux (as $L_u > L_d$), given by

$$R_{ln\ out}(t) = -R_{ln\ in}(t) \quad (B2)$$

Therefore, downward longwave radiation L_d [W/m²] is given as

$$L_d(t) = L_u(t) - R_{ln\ out}(t) \quad (B3)$$

with net outgoing longwave radiation $R_{ln\ out}$ [W/m²] given by (Allen et al. 1998; Jensen, Wright, and Pratt 1971; Shuttleworth 1992; J L Wright and Jensen 1972; James L Wright 1982)

$$R_{ln\ out}(t) = f(t)R_{ln0\ out}(t) \quad (B4)$$

where the net outgoing longwave radiation for a clear sky $R_{ln0\ out}$ [W/m²] is given by (Allen et al. 1998; Brunt 1932; Jensen, Wright, and Pratt 1971; J L Wright and Jensen 1972; James L Wright 1982)

$$R_{ln0\ out}(t) = (1 - \varepsilon_{a0}(t))\sigma(T_a(t) + 273.15)^4 \quad (B5)$$

Where the surface emissivity ε is assumed 1, and ε_{a0} [-] is the atmospheric emissivity for a clear sky (Brutsaert 1975) calculated from actual vapour pressure e_a [mbar] and daytime air temperature [°K]

$$\varepsilon_{a0}(t) = 1.24 \left(\frac{e_a(t)}{T_a(t)} \right)^{\frac{1}{7}} \quad (B6)$$

Or equivalently (with some truncation) after the units of vapour pressure e_a [Pa] and daytime air temperature [°C] have been changed.

$$\varepsilon_{a0}(t) = 0.65 \left(\frac{e_a(t)}{T_a(t) + 273.15} \right)^{0.14} \quad (B7)$$

And f (-) is a cloudiness factor (Allen et al. 1998; Jensen, Wright, and Pratt 1971; Shuttleworth 1992; J L Wright and Jensen 1972; James L Wright 1982)

$$f(t) = 1.35 \frac{K_d(t)}{K_{d0}(DOY)} - 0.35 \quad (B8)$$

with DOY [-] the numeric day of the year

With K_d [MJ/m²/day] downward shortwave radiation, and K_{d0} [MJ/m²/day] downward shortwave radiation for a clear sky, given as (Dong et al. 1992; Donohue, McVicar, and Roderick 2009; Liu and Jordan 1960):

$$K_{d0}(DOY) = \tau_0 R_a(DOY) \quad (B9)$$

where R_a (MJ/m²/day) is extraterrestrial radiation, and the atmospheric transmissivity for a clear sky τ_0 (-) for the southern hemisphere is (Roderick 1999)

$$\tau_0 = 0.8 \quad (\text{B10})$$

while a value of 0.7-0.75 could be used for the northern hemisphere (Roderick 1999).

The extraterrestrial radiation R_a [MJ/m²/day] is given by (Allen et al. 1998; Duffie and Beckman 2013; Iqbal 1983; Liu and Jordan 1960; Shuttleworth 1992)

$$R_a(DOY) = \frac{24}{\pi} I_{SC} E_0(DOY) (\omega(DOY) \sin \phi \sin \delta(DOY) + \cos \phi \cos \delta(DOY) \sin \omega(DOY)) \quad (\text{B11})$$

where I_{SC} [kJ/m²/h] is the solar constant (4921 kJ/m²/h or 1367 W/m²) (Fröhlich and Brusa 1981; Iqbal 1983) and E_0 (-) is the eccentricity correction factor of the Earth's orbit (around the sun) (Allen et al. 1998; Duffie and Beckman 2013; Iqbal 1983)

$$E_0(DOY) = 1 + 0.033 \cos\left(\frac{2\pi DOY}{365}\right) \quad (\text{B12})$$

Substituting the values for the atmospheric transmissivity for a clear sky τ_0 (-) and the solar constant I_{SC} [kJ/m²/h] gives

$$K_{d0}(DOY) = \frac{94.5}{\pi} E_0(DOY) (\omega(DOY) \sin \delta(DOY) \sin \phi + \cos \delta(DOY) \cos \phi \sin \omega(DOY)) \quad (\text{B13})$$

where ω [radians] is sunset hour (Allen et al. 1998; Iqbal 1983; Liu and Jordan 1960; Shuttleworth 1992), given by

$$\omega(DOY) = \cos^{-1}(-\tan \phi \tan \delta(DOY)) \quad (\text{B14})$$

with ϕ [radians] latitude, and δ (radians) solar declination calculated as (Iqbal 1983; Spencer 1971)

$$\delta(DOY) = 0.006918 - 0.39912 \cos \Gamma(DOY) + 0.070257 \sin \Gamma(DOY) - 0.006758 \cos 2\Gamma(DOY) + 0.000907 \sin 2\Gamma(DOY) - 0.002697 \cos 3\Gamma(DOY) + 0.00148 \sin 3\Gamma(DOY) \quad (\text{B15})$$

where Γ [radians] is the day angle, given by Iqbal (1983) as

$$\Gamma(DOY) = 2\pi \frac{(DOY-1)}{365} \quad (\text{B16})$$

The day length N [h] can be calculated from the sunset hour ω (radians) as (Duffie and Beckman 2013; Iqbal 1983; Shuttleworth 1992)

$$N(DOY) = 2\omega(DOY) \frac{24}{2\pi} \quad (\text{B17})$$

From which the daily fraction of daylight hours f_{day} [-] is computed

$$f_{day}(DOY) = \frac{N(DOY)}{24} \quad (\text{B18})$$

Therefore, the net outgoing longwave radiation $R_{ln out}$ is

$$R_{in\ out}(t) = \sigma(T_a(t) + 273.15)^4 \left(1 - 0.65 \left(\frac{e_a(t)}{T_a(t)+273.15}\right)^{0.14}\right) \left(1.35 \frac{K_d(t)}{K_{do}(DOY)} - 0.35\right) \quad (B19)$$

Which is similar to the net outgoing longwave radiation of Allen et al. (1998), but with different parameterisations for the atmospheric emissivity for a clear sky and daytime air temperature (and downward shortwave radiation for a clear sky).

Finally, the downward longwave radiation L_d [W/m²] can be represented as:

$$L_d(t) = \sigma(T_a(t) + 273.15)^4 - f(t)(1 - \varepsilon_{a0}(t))\sigma(T_a(t) + 273.15)^4 \quad (B20)$$

or

$$L_d(t) = \sigma(T_a(t) + 273.15)^4 \{1 - [1 - \varepsilon_{a0}(t)]f(t)\} \quad (B21)$$

or after substitution

$$L_d(t) = \sigma(T_a(t) + 273.15)^4 \left\{1 - \left[1 - 0.65 \left(\frac{e_a(t)}{T_a(t)+273.15}\right)^{0.14}\right] \left(1.35 \frac{K_d(t)}{K_{do}(DOY)} - 0.35\right)\right\} \quad (B22)$$

This is similar to the equation for L_d in Donohue et al. (2009), but with different parameterisations for the atmospheric emissivity and transmissivity for a clear sky.